UC San Diego
UC San Diego Electronic Theses and Dissertations

Title

Constructions of 2D-3D bio-mimetic DNA nanostructures

Permalink

https://escholarship.org/uc/item/0x66825f

Author

Xie, Sibai

Publication Date

2021

Peer reviewed|Thesis/dissertation

UNIVERSITY OF CALIFORNIA SAN DIEGO

Constructions of 2D-3D bio-mimetic DNA nanostructures

A dissertation submitted in partial satisfaction of the

requirements for the degree Doctor of Philosophy

in

Materials Science and Engineering

by

Sibai Xie

Committee in charge:

    Professor Yi Chen, Chair
    Professor Karen L. Christman
    Professor Darren J. Lipomi
    Professor Donald J. Sirbuly
    Professor Liangfang Zhang

2021

The Dissertation of Sibai Xie is approved, and is acceptable in quality and form for publication on microfilm and electronically.

University of California San Diego

2021

DEDICATION

To my mother, Qun Chen

Sibai Xie

TABLE OF CONTENTS

LIST OF FIGURES

ACKNOWLEDGEMENTS

I would like to first give my deepest appreciation to my advisor, Prof. Yi Chen, for his continuous support and guidance on my research during my Ph.D. study. He modeled for the whole lab with his work ethic and passion for research.

I also greatly appreciate all my committee members, including: Prof. Karen Christman, Prof. Darren Lipomi, Prof. Donald Sirbuly and Prof. Liangfang Zhang. I'd like to thank Prof. Christman for the insight and guidance she provided during my senate exam. I'm grateful that I had the chance to take Prof. Lipomi's class on intermolecular and surface forces, which helped me understand the dynamic aspects of my own research later on. I'm thankful for the collaboration with Prof. Sirbuly's lab and learning about nanowires, expanding my scope of possible applications of my research. Prof. Zhang opened the door of nanomedicine with his class I took, and facilitated the connection between Prof. Chen and I, and I am thankful for his guidance on my research direction.

Support from my family in China is critical to my study in the U.S. I am deeply grateful for the financial and emotional support from my mother, Qun Chen, over the 8 years I have been at UCSD, and throughout my entire life. I could not possibly make this long journey without the security she provided me along the way. Her understanding and patience were what supported me through the hardest times of my study away from home.

I am also grateful for the support from my friends and chosen family here in the US, in particular, Craig Jackson, Mark Thomas, and Jon Eikel. It has not been easy to establish a life and study towards a doctoral degree at the same time on a foreign land. They have helped through the

hardest times with love and support, have always been there for me, and are my role models in different aspects of life.

I'd also like to thank my current and former lab mates. Xiangyi Dong has provided with me tremendous support during the last couple years, with discussions on new projects ideas and also on graduation in general. When Dr. Chava Angell was a lab member, we had great discussions on each other's projects, and she helped me a lot on specific parts of my projects. Mingxuan Kai has also provided support as a lab mate.

VITA

2021   Ph.D. Materials Science and Engineering

        University of California San Diego, La Jolla, CA, USA

        Dissertation: Constructions of 2D-3D bio-mimetic DNA nanostructures

        Advisor: Professor Yi Chen

2013   M.S. Polymer Science

        University of Akron, Akron, OH, USA

2012   B.E. Chemical Engineering

        Suzhou University, Suzhou, China

PUBLICATIONS

S Xie, X Dong, Y Chen*, "2D-3D reversible transition of DNA nanostructures", *submitted*

S Xie, Y Chen*, "Cell membrane-mediated self-assembly of DNA nanostructures", *submitted*

C Angell, M Kai, **S Xie**, X Dong, Y Chen*, "Bioderived DNA Nanomachines for Potential Uses in Biosensing, Diagnostics, and Therapeutic Applications." *Advanced Healthcare Materials*, **2018**, *7*, 1701189

B Esteban-Fernández de Ávila, C Angell, F Soto, M.A. Lopez-Ramirez, D.F. Báez, **S Xie**, J Wang, Y Chen "Acoustically Propelled Nanomotors for Intracellular siRNA Delivery", *ACS Nano*, **2016**, *10(5)*, 4997-5005

C Angell, **S Xie**, L Zhang, Y Chen* "DNA Nanotechnology for Precise Control over Drug Delivery and Gene Therapy", *Small*, **2016**, 12(9), 1117-1132 (co-first author)

F Lin, J Yu, W Tang, J Zheng, **S Xie**, M L Becker* "Postelectrospinning "Click" Modification of Degradable Amino Acid-Based Poly(ester urea) Nanofibers", *Macromolecules*, **2013**, *46(24),* 9515–9525

W Tang, Y Ma, **S Xie**, K Gao, B Katzenmeyer, C Wesdemiotis, ML Becker* "Valency-Dependent Affinity of Bioactive Hydroxyapatite-Binding Dendrons", *Biomacromolecules*, **2013**, *14(9)*, 3304-3313

LA Smith Callahan, **S Xie**, I Barker, J Zheng, DH Reneker, AP Dove, ML Becker* "Directed differentiation and neurite extension of mouse embryonic stem cell on aligned poly(lactide) nanofibers functionalized with YIGSR peptide" *Biomaterials,* **2013***, 34(36),* 9089–9095

T Rao, G Singh, **S Xie**, A Karim*, ML Becker* "2-D gold nanoparticle arrays from thermally directed self-assembly of peptide-derivatized block copolymers" *Soft Matter*, **2013**, *9,* 8023-8032

J Zhou, **S Xie**, EF Amond*†*, ML Becker* "Tuning Energy Levels of Low Bandgap Semi-Random Two Acceptor Copolymers" *Macromolecules*, **2013**, *46(9),* 3391-3394

J Zheng, **S Xie**, F Lin, G Hua, T Yu, DH Reneker, M L Becker* "Dibenzocyclooctyne as an Initiator for Poly(e-caprolactone): Copper-Free Clickable Polymer and Nanofiber Based Scaffolds" *Polymer Chemistry*, **2013**, *4(7)*, 2215-2218. *– featured on journal cover, created the cover illustration*

S Cheng, X Li., **S Xie**., Y Chen, L-J Fan* "Preparation of electrospun luminescent polyimide/europium nanofibers by simultaneous in situ sol–gel and imidization processes" *Journal of Colloid and Interface Science* **2011**, *356*, 92–99

ABSTRACT OF DISSERTATION

Constructions of 2D-3D bio-mimetic DNA nanostructures

by

Sibai Xie

Doctor of Philosophy in Materials Science and Engineering

University of California San Diego, 2021

Professor Yi Chen, Chair

DNA nanotechnology as a versatile tool has been growing rapidly in the past three decades, with applications across different disciplines such as drug delivery, imaging, and even computing. Its versatility stems from the programmable nature of DNA and the ability to self-assemble through the A-T and C-G base pairing by hydrogen bonds. These features make DNA nanotechnology the ideal tool for mimicking and studying biological processes that are hard to otherwise model. In this work, the process we focus on is Clathrin-Mediated Endocytosis (CME). CME is one of the major mechanisms for cell entry. This pathway internalizes Influenza A, vesicular stomatitis virus,

and many others. Mimicking this process will help us further understand it, and also find ways to utilize it in the field of drug delivery.

The process of CME can be described in 3 major steps. The first step is array formation. Clathrin can cluster on cell surface in the form of triskelion, to form small patches of an array. The second step involves the recruitment of adaptor proteins, that transforms the array into three-dimensional lattices to encapsulate the foreign agent. The third step is the transportation of the vehicle inside the cell, along with the disassembly of the vehicle to release the agent.

Specifically for each stage, we designed mimicking mechanisms using DNA nano-structures. For the array stage, we designed a three-point-star motif to mimic the triskelion structure, and functionalized it with cholesterol to integrate the array to the cell membrane. Characterization through liquid atomic force microscopy (AFM) showed clear hexagonal pattern, and *in vitro* cell experiment also showed the integration of the arrays to cell membranes. For the transition stage, we designed a reversible 2D-3D transition mechanism that allowed the 2D arrays to transform into 3D particles with the addition of a particular stimuli, that is a DNA single strand. The transformability and reversibility were confirmed through polyacrylamide gel electrophoresis (PAGE), dynamic light scattering (DLS) and AFM. For the delivery stage, we designed several 3D DNA structures for better drug delivery efficiency, and the designs were also characterized by PAGE and AFM.

The successful designs for all three stages led us closer to understanding the structural transformation of clathrin triskelion during CME. The 2D-3D transition mechanism also has the potential to be used in other systems, such as stimuli-controlled drug release and DNA computing using single strand DNA.

CHAPTER 1: INTRODUCTION AND OBJECTIVES

1.1   DNA nanotechnology

Deoxyribonucleic acid, commonly abbreviated as DNA, is the genetic information carrier for most life forms on earth. Because of its ability to self-assemble, it has been used as a material to construct nanoscale structures for varies applications in the past three decades. In this chapter, we briefly review key developments of the field of DNA nanotechnology, and how they have led to our objectives of mimicking clathrin-mediated endocytosis in different stages.

DNA nanotechnology as a versatile tool has grown rapidly in the past three decades, especially for its use for precise control over drug delivery[1]. The technology utilizes the programmable self-assembly of DNA to construct nanoscale features that can be easily modified and functionalized.

The general procedure for the successful synthesis of a DNA nanostructure would include three phases: Design, hybridization, and characterization.

For the design phase, a few basic principles were presented by Ned Seeman[2]. Some software has been used for the design purposes, such as caDNAno for DNA origami design[3]. Figure 1-1 shows the design interface. The software integrates the design principles, and gives suggestions to improve stabilities of the final structures. Aside from using software, the sequences of DNA strands are often presented in a 2D view, where each line represents a single strand (Figure 1-2). A series of DNA sequences will be generated after the design process. The synthesis of these strands is usually done by companies that specialize in DNA synthesis for the sake of efficiency. The strands are purified after arrival for use in the next step – hybridization.

In the hybridization phase, purified DNA strands are mixed together with precisely controlled stoichiometry in a buffer, usually with a certain concentration of free magnesium ion.

The solution then undergoes a gradual temperature decrease process that is called annealing. The temperature range is usually 95 °C to 4 °C, in a time period ranging from 48 hours [ref] to 30 seconds[4], depending on the design and size of the desired structure. For example, a larger structure such as array would require overnight annealing, while smaller structures like triangles or tetrahedrons would require only a few hours. The purpose of this process is to allow the structures to gradually settle into the minimal energy equilibrium states, which are the structures that are originally designed for, and avoid the formation of semi-stable intermediate states, especially in the case of larger structures.

The characterization phase is critical for validation of the design. The design principles are nowhere near comprehensive, thus there is a significant chance that unaccounted interactions or secondary structures may occur. A major problem in the design is excess symmetry. This will be further discussed in chapter 5.3. Common characterization methods include denature/native PAGE, agarose gel electrophoresis, Atomic Force Microscopy (AFM) either in air or in liquid, optical/florescent microscope, Dynamic Light Scattering (DLS), Cryogenic electron microscope, etc. These methods are used to confirm the sizes or changes in sizes of the structures, the shape and the morphology, and specific characteristics such as fluorescence. It is important to use several of these methods to confirm the formation of the structure, as well as confirm the occurrence of purposed mechanism. Often, the characterizations don't go as expected. A debugging process is required after that in order to refine the design for the purpose of the experiment, and go through the whole process again until the goal is met.

The rest of Chapter 1.1 will focus on major fabrication principles and applications.

Figure 1-1 Interface of caDNAno, a software for designing DNA origami sequences. Left panel, A cross-sectional view of possible helices position within a honeycomb lattice. Middle panel, 2D schematic for the design of staple paths within the DNA scaffold. Right panel, Real-time 3D rendering of the design[3].

Figure 1-2 A sample figure for 2D view of a DNA nanostructure design. The arrow indicates the direction of the strand from 5' end to 3' end. The actual sequences of the strands are simplied to lines for simplicity when demontrating the shape of the design.

1.1.1 Tile Approach

Since Ned Seeman proposed an immobile four-way junction in 1983[2], this particular mechanism has been used to construct DNA nanostructures. Tile approach is one of the earliest categories that are generally used as design principles. Tiles typically consist of a few short (up to 150 nt) DNA single strands, and there are usually sticky-ends at the edges of the tiles in order for them to link to each other. A typical example would be a 3-point-star motif[5]. With as few as 3 strands, a 3-arm motif is formed with sticky ends at the terminals of each strand. These ends can hybridize with other ends strongly enough to form different structures, such as tetrahedron, dodecahedron and buckyball, by fine-tuning the number of unpaired bases at the turning points of the central strands[6] (Figure 1-3). The same group used a similar approach to create a 5-point-star motif, and they discovered that under optimal concentration, the tiles can form a truncated icosahedron structure[7] (Figure 1-4).
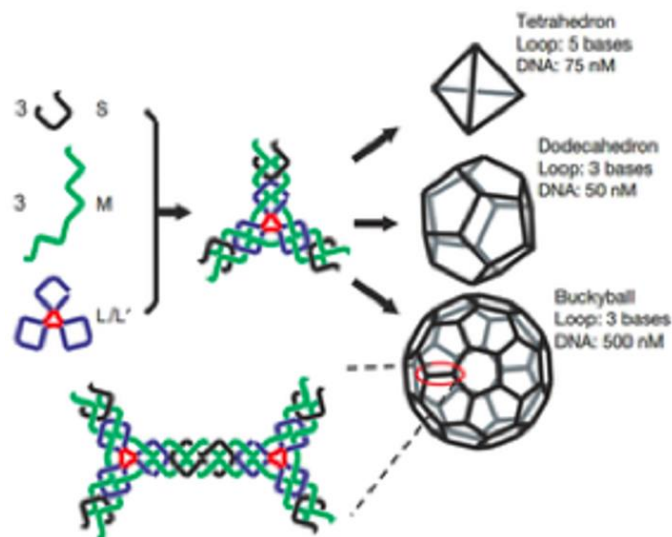
Figure 1-3 Different structures formed by the same three-point-star motif with different "loop" length and concentration.[6]
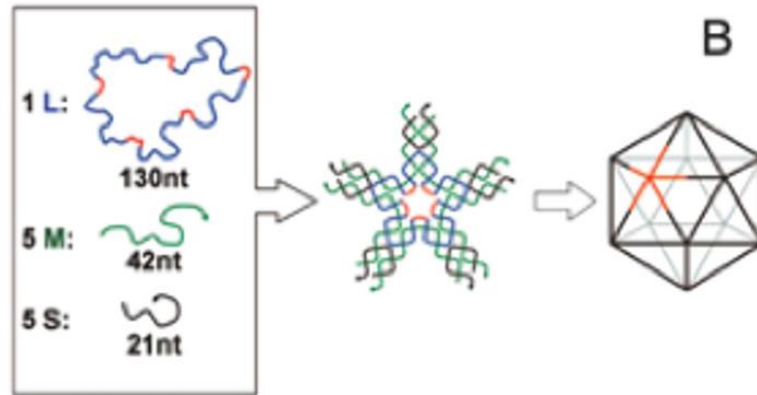
Figure 1-4 Icosahedral structure formed by flexible five-point-star motifs[7].

Another type of tile is described by Ke *et al*. In 2012, they reported the construction of short "DNA bricks" that can be used to create many different types of structures without having to redesign staple strands and scaffolding routing as is necessary in creating varying origami structures (Figure 1-5)[8]. The authors reported essentially a lego-like modality in which each brick had a distinct shape and could bind to 4 neighbors just as a lego can fit into specific holes. These interactions are defined by the domains of the DNA bricks which have unique sequences. Therefore, each 32-nucleotide brick is distinctive and can be combined to create different 3D structures with both controllable surface features and precise cavities within the structure. 102 different structures were created using this method merely by selecting the bricks needed which greatly simplifies the process of creating 3D DNA nanostructures[8].
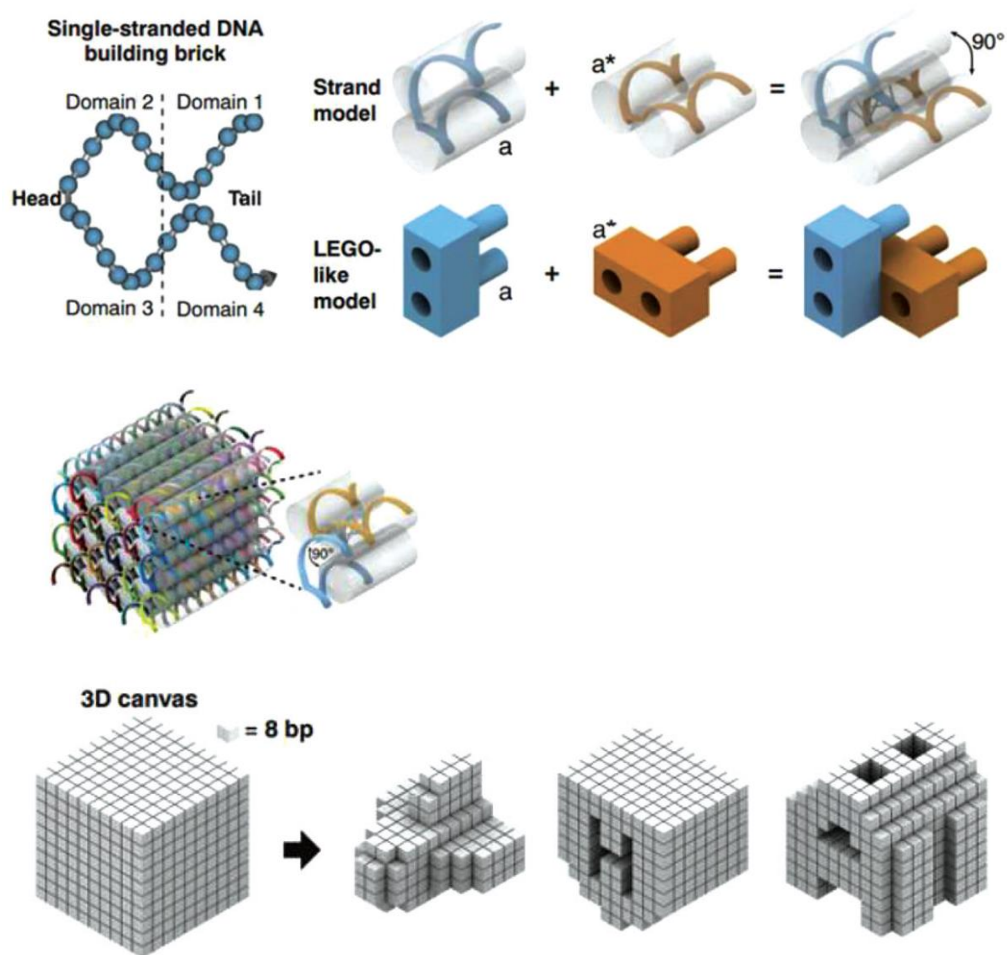
Figure 1-5 Single-stranded DNA bricks form 3D canvas, and the canvas can be carved into different shapes[8].

Some other designs don't involve repeated tile structures, but they are similar in the sense that each motif is constructed by the same few DNA single strands.

Goodman *et al.* reported a facile way of building DNA tetrahedra using four different strands, with the struts less than 10 nm in length[4]. Under the simple process of cooling from 95 °C to 4 °C in 30 s, tetrahedra form under a yield of 95% and can be characterized by a single band on a native gel.

DNA nanostructures can also be formed through a step-by-step process. Chen *et al.* demonstrated this method by constructing a nano-scale cube structure (Figure 1-6)[9]. In each step they hybridize two squares and in the last step the ends are connected to form a cube.
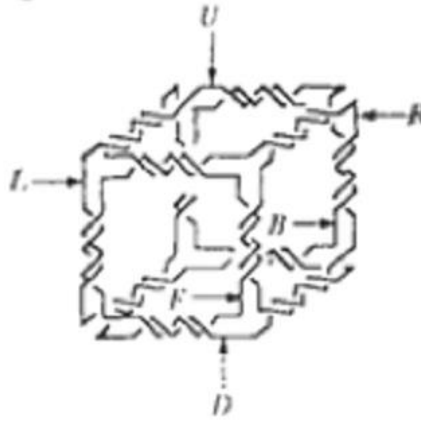
Figure 1-6 Truncated cubic structure[9].

The above examples of various tile approaches indicate that this is a powerful and versatile method to construct DNA nanostructure, be it arrays, truncated particles, or more complicated structures. The major design principle used in this dissertation work is tile approach, for the design simplicity and versatility. The design details will be discussed in chapters 2-4.

1.1.2 Origami Approach

Other strategies for synthesizing precision DNA nanotechnology are also extremely attractive for their shape control, control of flexibility and size, and ability to create larger, modular structures that can even be extended to include kinematic, movable joints[10–13]. This approach is normally called DNA origami. It was pioneered by Paul Rothemund in 2006 (Figure 1-7)[10]. DNA origami refers to the folding of a long-stranded bacteriophage (7240 nt) through the use of over 200 complementary staple strands to fold the backbone. Paul Rothemund used the M13m18 bacteriophage and his original structures were 2D. Each oligonucleotide is considered a 6 nm pixel to build any pattern of desire. By putting sticky ends on the connection part of each construct, an extended array can also be formed. Since then, the DNA origami motif has been extended to three dimensions[3,11].
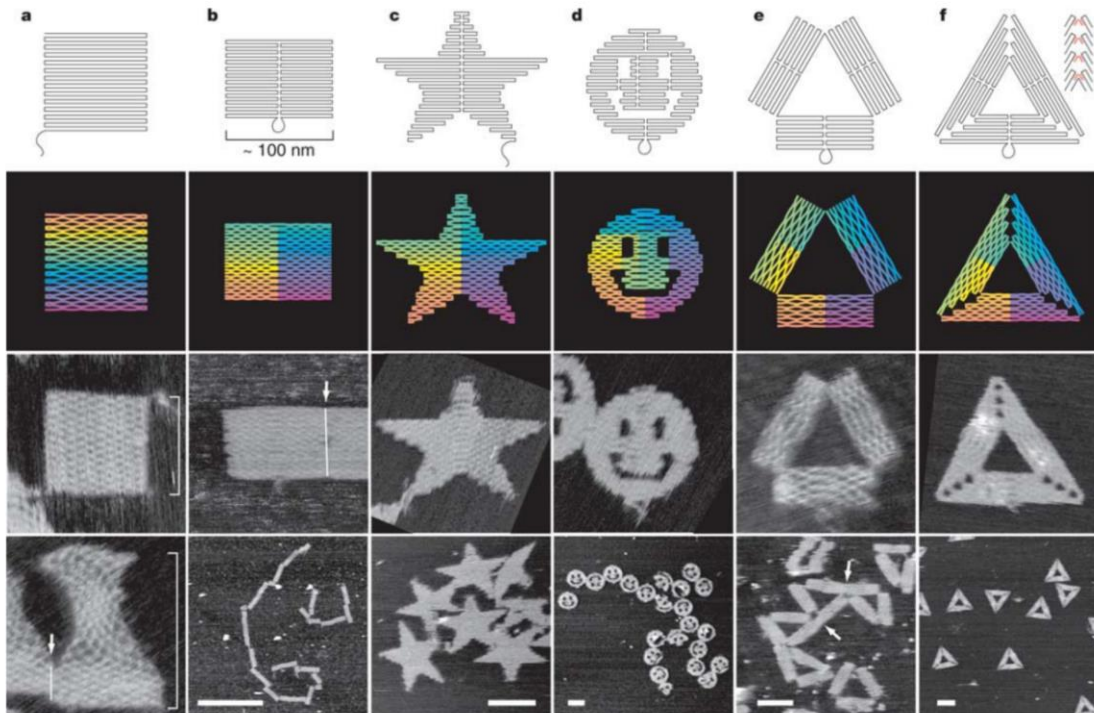
Figure 1-7 Rothemund's DNA origami shapes.

Because these structures are based on a long backbone structure and hundreds of staple strands, the design process can be time consuming. Thus, there are now several computer programs that facilitate the design of DNA origami structures such as caDNAno and SARSE[14,15]. With DNA origami, structures such as smiley faces, tetrahedrons, DNA nanotubes, DNA barrels, DNA "dolphins" and many other shapes are possible[10,12,16–18]. Many groups have worked on extending this modality and facilitating its use for structural formation and drug delivery.
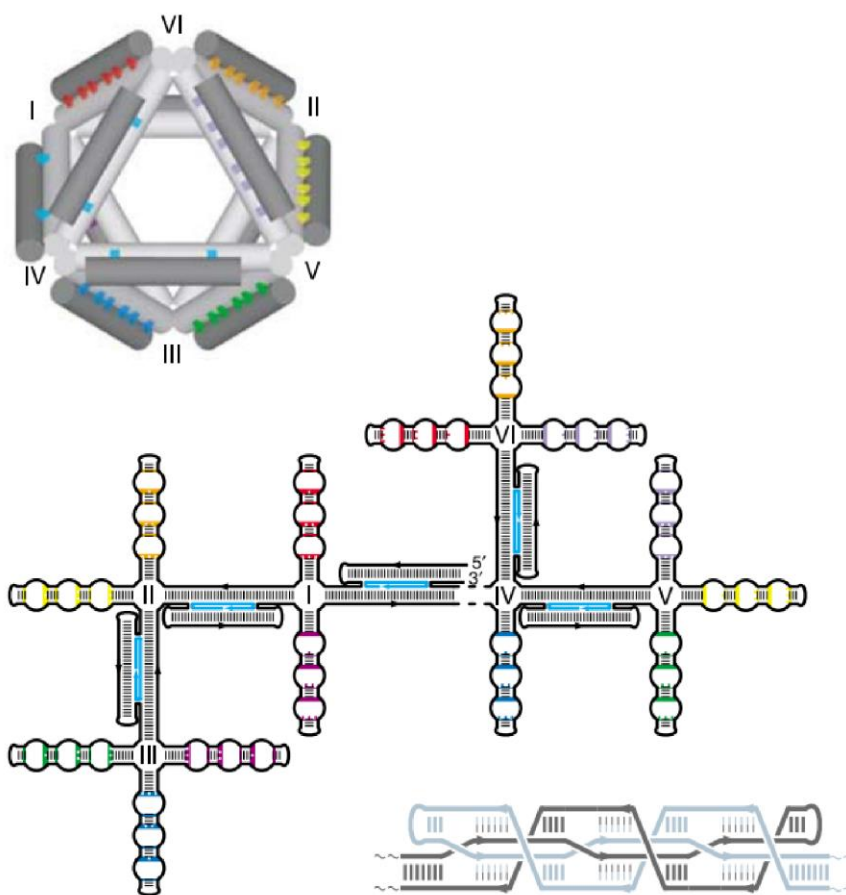
Figure 1-8 DNA octahedron obtained by folding a 1.7 kilobase backbone[14].

Shih *et al.* reported back in 2004 an idea similar to the later developed DNA approach, which is to fold a long backbone DNA chain by binding it at different points using staple strands (Figure 1-8)[14]. In this example a 1669-nucleotide single-stranded DNA is used as the backbone and five 40-nucleotide strands are used to fold the backbone. Double-crossover and paranemic-crossover structures are designed to ensure the stiffness of the structure. It was proposed that the long backbone chain can be readily amplified. Douglas *et al.* reported that using the same DNA origami method, it is also possible to fabricate 3D structures[11]. They used honeycomb-pleat based strategy to bring the helices together at a certain angle to construct 3D structures (Figure 1.4 C). They also developed a software called caDNAno, an easy tool to design 3D structures and program the staple strands[3]. The whole design and synthesis process took 2 weeks as they reported. One of the largest challenges that faced DNA origami was the time it takes to fold and hybridize the structures. In 2012, Sobczak *et al.* determined that a long annealing process is not necessary to create these structures in a "one-pot" reaction scheme as there is a distinct range where DNA will fold and hybridize[19]. These experiments also reported that DNA folding and unfolding are non-equilibrium processes as the temperature for unfolding is higher than the one at which the structures formed. This experiment allows DNA origami to be formed on a more feasible time scale.
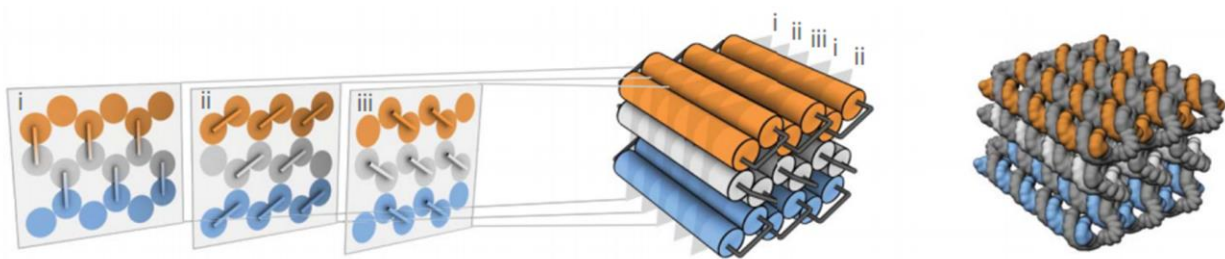
Figure 1-9 3D DNA origami structures using honeycomb-pleat based strategy[11].

There is a desire within this field to create large structures that mimic viral capsids, which is a similar goal to the one in Chapter 4. Iinuma *et al.* reported the construction of polyhedra from million daltons (MD) monomers (Figure 1-10)[20]. These monomers created a 5-MD DNA origami three arm junction that was sixty times more massive than previously reported 3-arm motifs. These junctions have a "dynamic connector" design and Iinuma *et al.* created a DNA tetrahedron, a cube, a triangular prism, a pentagonal prism, and a hexagonal prism. All structures were on the order of 20–60 MD and had compartments that are similar in size to those of bacterial microcompartments and could be used to carry therapeutic loads.
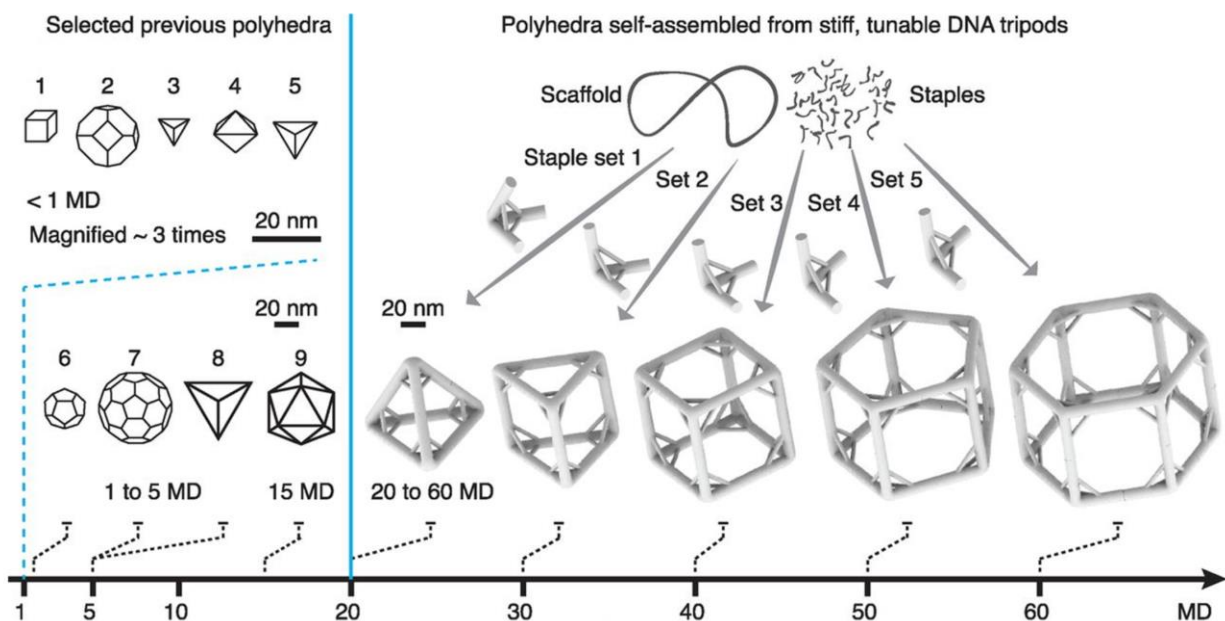
Figure 1-10 Large 3D structures synthesized to carry therapeutic loads[20].

Compared to tile approach, the origami strategy is more suitable for larger more complicated structure. It has the potential to expend our scope on the bio-mimetic process described in this work.

1.2 Clathrin-Mediated Endocytosis and DNA nanotechnology

Endocytosis is the process where the cells uptake extracellular materials. Thus, this process is vital to the survival of cells. There are different mechanisms where endocytosis could occur. clathrin-mediated endocytosis (CME) is one of them.
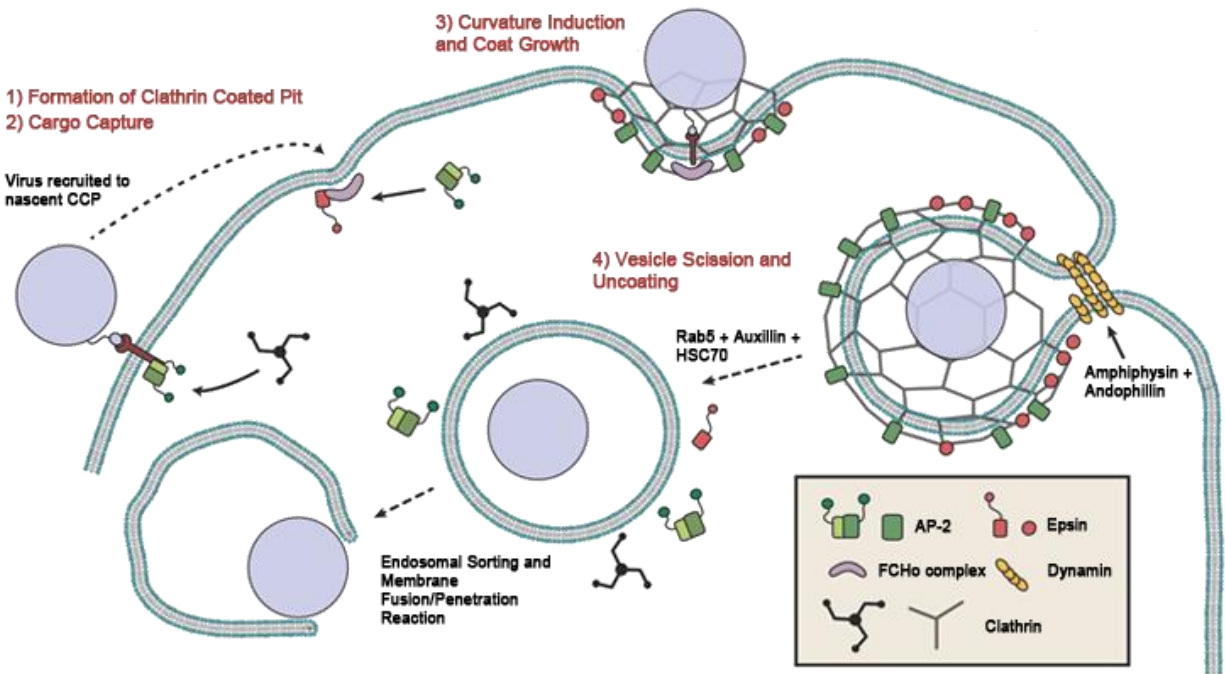
Figure 1-11 Process of Clathrin mediated endocytosis[21].

Clathrin is a critical protein involved in the process of CMEC[21]. This process involves a number of proteins. To briefly summarize the process, a viral entry is used as an example in Figure 1-11.

Before the virus engages with the receptor, clathrin coated-pits (CCPs) are formed on the surface of the cell membrane by FCHo complex, which contains a curvature inducing F-BAR dimer for the initial formation of the curvature[22]. The FCHo complex recruits Eps15 and Epsin which recruits AP-2 to the membrane[23], and AP-2 is one of the critical adapter proteins that help form the clathrin lattice. The clathrin triskelia polymerize to form a lattice on the membrane, once the concentration of clathrin reaches a critical level[24].

Once a cargo (virus particle) is captured by a cross-membrane receptor, the receptor will bind to AP-2 as well. This cargo-receptor-AP-2 complex is then recruited to an adjacent site of nascent CCP. AP-2 continues to recruit clathrin onto the CCP, eventually increasing the clathrin concentration so that the triskelia polymerize and form a lattice on the membrane in a basket shape. A region of tubular neck will be formed that is uncovered by clathrin.

This neck region will attract amphiphysin and endophilin. After binding with dynamin, amphyphysin polymerizes along the neck into a helical collar, and eventually scissor the vesicles off the membrane. The clathrin-coated vesicle is now in the cytoplasm. Auxillin and Hsc70 then come in to disassemble the clathrin coat.

Although the process of CME has been understood in detail as described above, there are still parts that require further understanding. One key part is whether the clathrin patches form large arrays on the surface of the cell membrane first and then fold into 3D vesicles, or the clathrin triskelion nuclearize based on a small clathrin patch and form curvature from there[25]. Understanding this process would help us find better ways to deliver agents into cells.

This process is hard to directly observe under microscope because this is a dynamic process that happens in live cells. It is also difficult to recreate the process using exactly the proteins involved, for that there are a number of proteins active in this process, and some of the protein

interactions involve ATP. Thus, we need to find another model materials to mimic this process, and DNA nanotechnology is an ideal candidate.

There are many similarities between the CME process and what a DNA nanostructure system can achieve. One thing is the size. The heavy chain on clathrin is about 160 Å long with an oval cross section of 24×28 Å[26]. With DNA, we can constructure tunable arm lengths, and DNA double helix has a diameter of 20 Å. Clathrin has a non-covalently trimerized structure, and DNA hybridization is based on hydrogen bonding, with intra-strand and inter-strand π–π stacking, and other non-covalent interactions. DNA can mimic the stimuli-responsive nature of CME, by introducing structural strand to trigger conformational change, in comparison to CME regulated by accessory proteins.

Because of these similarities, we wanted to explore using DNA nanotechnology to make a model system to mimic CME.

1.3 Objectives

In order to mimic the process of CME, we simplified it into three stages: array, transformation, and delivery. We designed mechanisms that are specific to each stage of CME.

For the array stage, the goal is to create an array that is capable of self-assembly while being able to attach to the cell membrane. For these functionalities, we designed a 3-arm motif with stick ends and also an anchoring domain modified with cholesterol. The sticky ends ensure the self-assembly of the array and cholesterol in the anchoring domain attaches the array to cell membranes. The design and characterization will be discussed in detail in Chapter 2.

For the transformation stage, the goal is to design a reversible 2D-3D transformation mechanism that is mediated by certain stimuli. To do this, we took a two-step approach. In the first

step, we tested the mechanisms of fuel-strand replacement and hairpin expansion on a single motif design. The single motifs can respond to the addition of certain single strand DNA, and switch between 2D and 3D conformation. In the second step, we expanded the application of the same mechanisms to transform arrays to 3D particles. The designs and characterizations of these two designs will be discussed in detail in Chapter 3.

For the delivery stage, the goal is to design truncated DNA nanoparticles that can carry specific agents into the cell. We explored symmetric and non-symmetric design principles. This constitutes the major part of Chapter 4.

Figure 1-12 depicts each stage of CME and the corresponding design of DNA nanostructures.
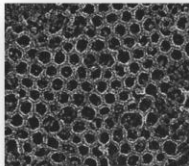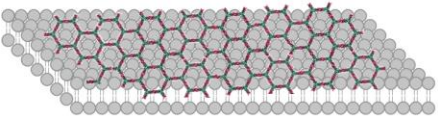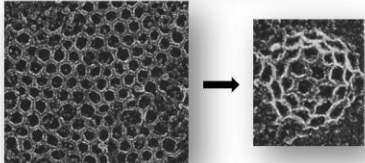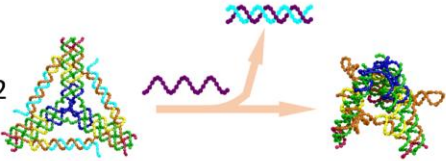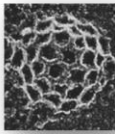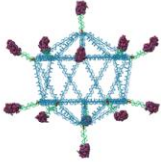
Figure 1-12 The stages of CME that we are trying to mimic with the corresponding DNA nanostructure designs.

Chapter 1, in part, is a reprint of the material as it appears in "DNA Nanotechnology for Precise Control over Drug Delivery and Gene Therapy", *Small*, **2016**, 12(9), 1117-1132, with the coauthors of C. Angell, L. Zhang, Y. Chen. The dissertation author is the co-first author of this work.

CHAPTER 2: Clathrin-Mimic DNA Arrays

2.1 Introduction

Cells utilize membrane-bound vesicles to transfer macromolecules in the secretory and endocytic pathways. These vesicles are classified according to the containing proteins. One of the most common classes of protein is clathrin. Clathrin mediated endocytosis is one of the most common way for cell to uptake exterior chemicals used by all known eukaryotic cells. This process also regulates surface proteins, signaling pathway and turning over membrane components. Similar as many other cellular functions and events, it starts from the assembly of membrane associated protein, in this case, triskelion, clustering. During the formation, adaptor proteins recruit clathrin and connect receptor. Triskelion can self-assemble into regular three-dimensional lattices, consisting both hexagons and pentagons. Triskelion is a protein complex has three arms in a threefold symmetry. In clathrin-mediated endocytosis, the arm of triskelion connects to another, results form a hexagonal and pentagonal array. When all the lattices are hexagonal, it will resist bending and forms the planar patches on cell surface. When mixed with pentagons, the flexibility introduces a membrane curvature on cell surface and thus resulting a vesicle for endocytosis.

Understanding and mimicking clathrin-mediated endocytosis could benefit many biomedical applications, such as nanoparticle-based drug delivery, which utilize such process to enter cell. However, satisfying such molecular precision requirement is challenging. Among all the available systems, DNA nanotechnology is the most promising platform because of the precisely controllable ability on nanometer scale. Fueled by base-pairing ability, DNA nanotechnology has enabled many strategies to form DNA nanostructures with well-defined structures. It has been proven to successfully construct one-dimensional nanowires, two-dimensional array and three-dimensional objects with nanometer precision. Currently, this

technology was also applied to understanding the cell membrane process by investigating the interactions between the membrane-mimic lipid bilayer and DNA nanostructures. It has been proved the formation of membrane-spanning channel, and polymerization of DNA origami nanostructures.

Here, we present an approach that uses DNA nanotechnology to mimic the clathrin patch self-assembly process on cell surface. We designed an array-forming 3-arm motif with sticky-ends, synthesized it and characterized the motif and array using gel electrophoresis, atomic force microscopy in fluid, and florescence microscopy.

2.2   Results and Discussion

Inspired by the triskelion self-assembly, we used a DNA 3-arm motif to mimic the structure and mechanism (Figure 2-1, 2-2). Similar as triskelion, the 3-arm motif has threefold symmetry and could self-assemble. To achieve similar functionalities, we used a center strand that has one single anchor strand domain and three identical arm domains. Since DNA strands are highly negatively charged entities, in order to bring DNA arrays onto cell surface, an anchoring strategy is needed. This anchor domain in the center strand can hybridize with cholesterol labeled single strand DNA that allows the motif to insert into membrane bilayer.
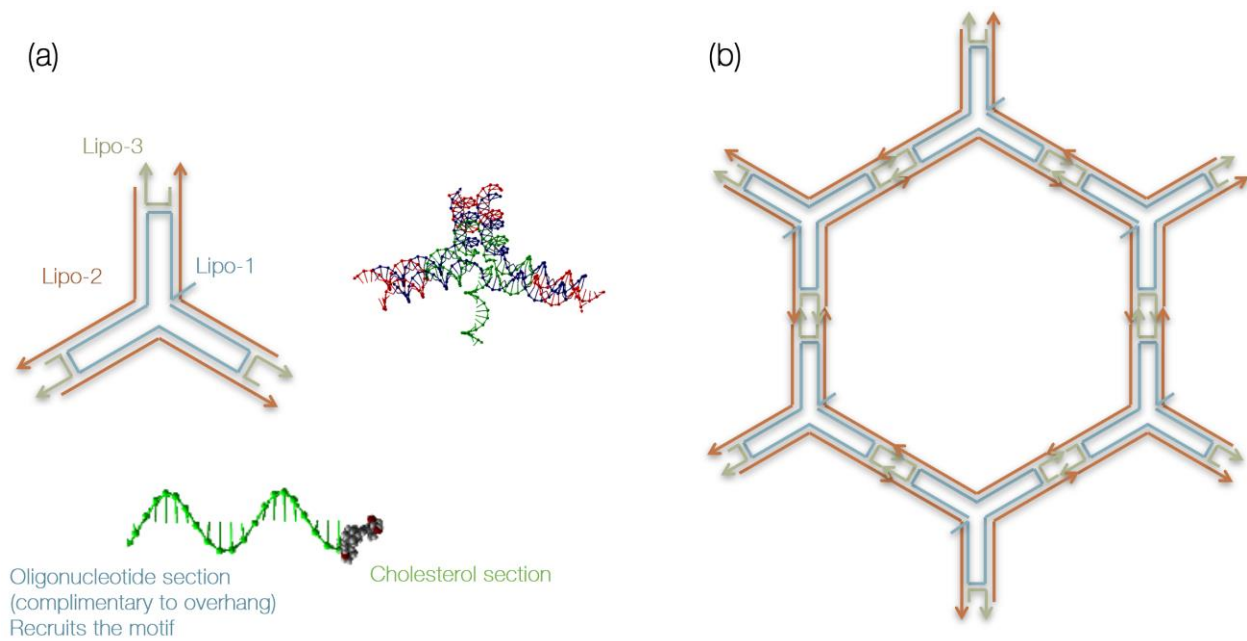
Figure 2-1 Schematic drawing of the clathrin patch mimicking DNA motifs. (a): Left: schematic drawing of the design, indicating different strands as lipo-1, lipo-2, lipo-3. Right: 3D rendering of the motif. Bottom: 3D rendering of the cholesterol modified oligonucleotide used as anchoring recruiting agent. (b): demonstration of how connecting the termini of each arms of the motif could form a hexagonal array.

The arm domains will bind with three arm strands and result in 3-arm motif. At termini of each arm, there are sticky-ends. Three linker strands, which will bind with arm strands and form the crossover structure with center strand, will provide the structure stability of the three-arm motif and act like the chains of triskelion that associate with each other to enable the further assembly process. This is shown in Figure 2-1 (b). The formation process of the array on the lipid memberane is shown in Figure 2-2. The cholesterol modified oligonugleotide is infused into the memberane coated on the mica surface first, and act as a recruiting agent to gather the pre-formed 3-arm motif onto the surface. The motifs then bind to each other by the sticky ends, and form a large array anchored into the lipid surface.
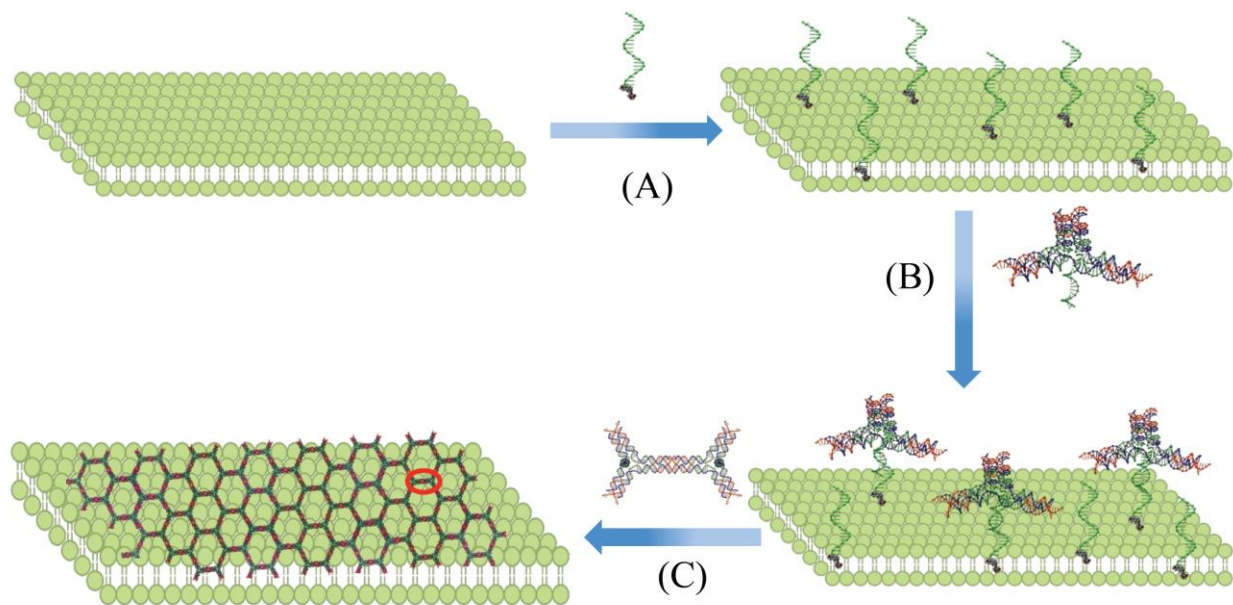
Figure 2-2 Schematic drawing of the clathrin patch mimicking DNA nanopatterns formation. (A)Cholesterol modified single DNA strands insert into lipid bilayer as anchor. (B) DNA single tile was first assembled in aqueous solution. This three-arm tile contains seven DNA strands: the center long single strand with three repetitive parts to form arms and with anchor part to hybridize the anchor strand on lipid bilayer, three identical arm strands that form two DNA duplexes with center strands, and three identical linker strands that form the crossover other duplex with two sticky ends parts to connect other tiles. (C) With the help of anchor strands diffusing, macro pattern DNA nanopatterns are formed on lipid bilayer.

The formation of motif and the array was first confirmed by polyacrylamide electrophoresis (PAGE) in native condition. In Figure 2-3, the gel image clearly shows each step of the motif formation. In Lane 6, the DNA sample stuck in the well, indicating the formation of a larger structure.
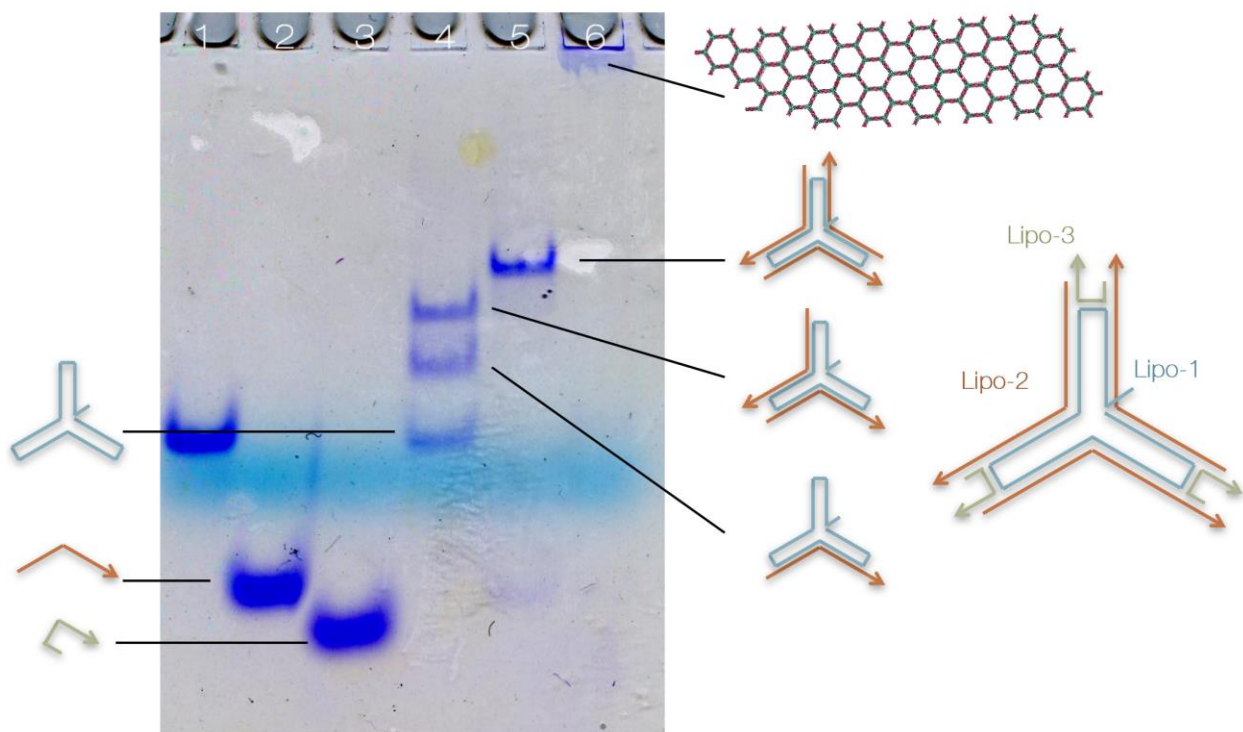
Figure 2-3 Native 8% PAGE gel for the characterization of the motif and the array. Lane 1-3: purified lipo-1, lipo-2, lipo-3 strands. Lane 4: 1:1 ratio of lipo-1 and lipo-2 combined. Because of the insufficient amount of lipo-2, different intermediate products were formed. Lane 5: 1:3 ratio of lipo-1 and lipo-2. Lane 6: 1:3:3 ratio of lipo-, lipo-2, lipo-3. The product stuck in the well.

We then tested our approach in a simplified cell membrane system, a supported lipid bilayer. Following tradition lipid bilayer formation, L-α-phosphatidylcholine from egg (Egg pc) was coated on mica surface. Then, the cholesterol labeled DNA single strands were mixed with lipid bilayer in buffer. Due to its hydrophobicity, the cholesterol inserted into bilayer and bring the linked DNA strands to lipid bilayer surface. The triskelion mimic DNA 3-arm motifs were formed by cooling down the single-stand-containing TAEMg buffer solution from 95°C to 60°C. At this relatively high temperature, the units could not readily associate with each other but instead would remain as individual motifs, but still strong enough to hybridize with the anchor strands. When these individual motifs were mixed with anchored lipid bilayer, the anchor strands would bind with individual single motifs, bring them to the membrane surface. Once these motifs were anchored onto the lipid surface, the sticky ends at each individual motif can start to self-assemble when temperature decrease. Due to the fluidity of lipid membrane, the anchor strand with cholesterol could move freely on it and facilitate the association of individual motifs and make them self-assemble into desired patterns.

After the assembly on lipid bilayer surfaces, the DNA nanopatterns were imaged directly by AFM (Figure 2-4). Clathrin patch mimicking hexagonal patterns are clearly visible. Such patterns are consistent with the molecular designs and are essentially the same as the patterns observed as clathrin patch. In the hexagonal array, the size of each struct is around 15 nm, which is comparable with the real clathrin patch.
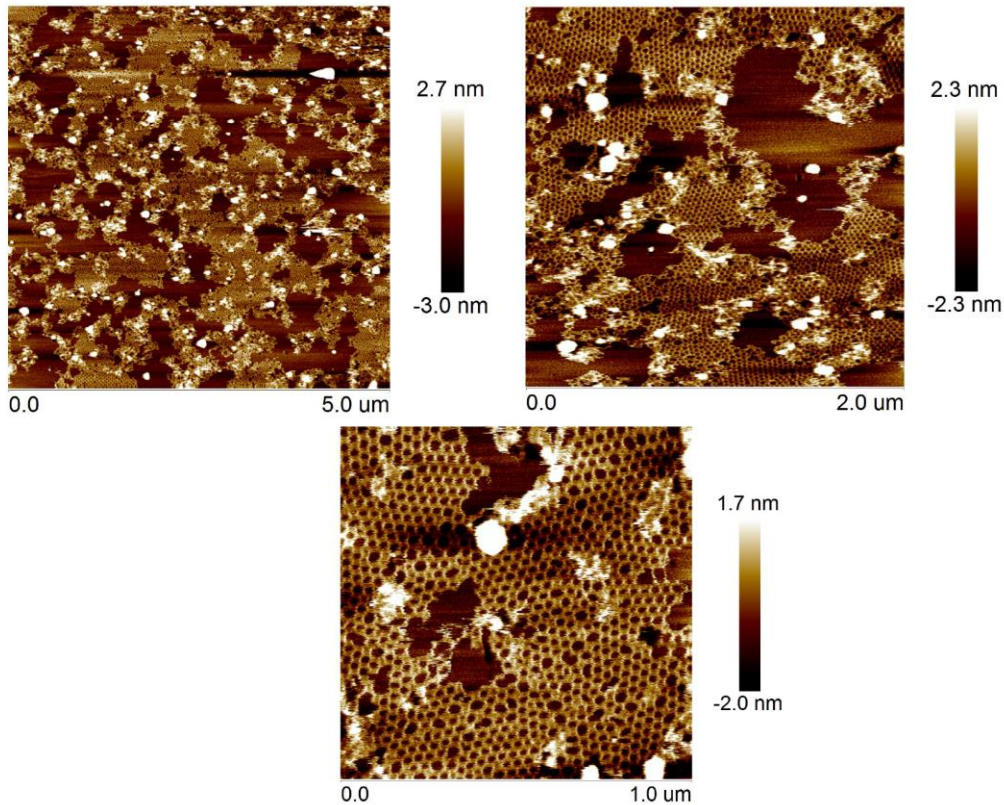
Figure 2-4 Atomic force microscopy (AFM) images of DNA 2D arrays on lipid bilayer with increased magnification. Anchor strands 10nt long.

The real cell membrane surface is a complicated system, covered by membrane protein, nucleic acid and carbohydrates, which would require the assembled system on top to have more depth capacities to tolerate the rugged surface morphology. In order to achieve the assembly on real cell membranes, we tested the different lengths of anchor strands that control the space between the array and membrane surface. We increased the anchor strand to 20 nt and 30 nt, corresponding to 7 nm and 10 nm respectively. When the distance is about 7 nm between the array and the membrane surface, we could still find the hexagonal arrays (figure 2-5A). However, when it goes up to 10 nm, the tiles will still attempt to associate with each other because the kinetic barrier is too high; but the assembled array will lose its rigidity because the space between the

23

array and lipid membrane is too high. Consequently, the hexagonal arrays will cover the whole area with multiple empty holes where the motifs dissociate with each other due to excess flexibility (Figure 2-6).
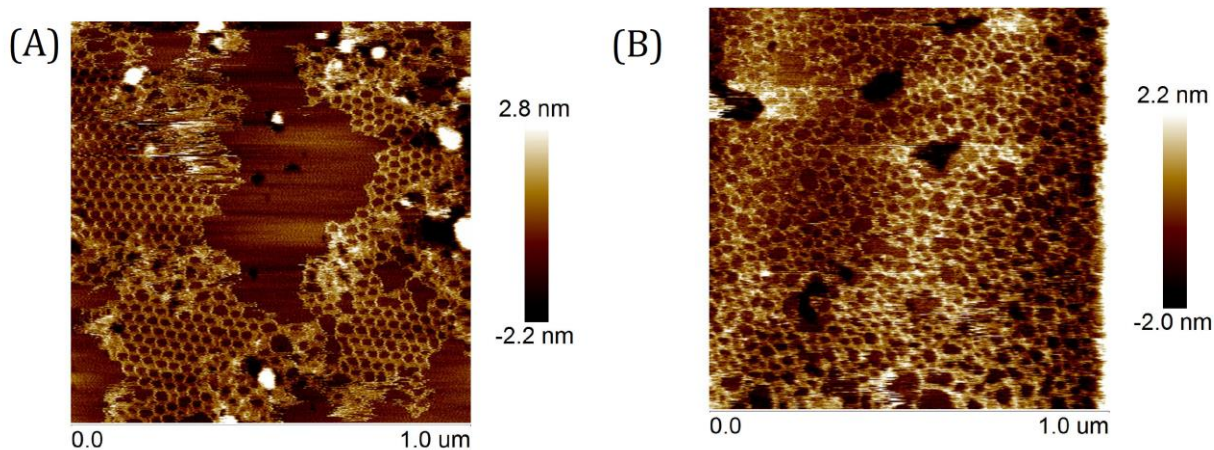
Figure 2-5 Atomic force microscopy (AFM) images of DNA 2D arrays on lipid bilayer with increased magnification. (A) anchor strands 20nt long (B) anchor strands 30 nt long.

As one possible approach to overcome the flexibility issue, we improved the density of the array. In principle, when the whole area is covered with DNA arrays, there is no room for the array to twist. What we expected to see will be a rigid array the same as the small distance condition. In Figure 2-6, when the concentration of single motif with 30nt length anchor strand was increased to eight times, the whole lipid bilayer was covered with rigid hexagonal arrays, as expected.
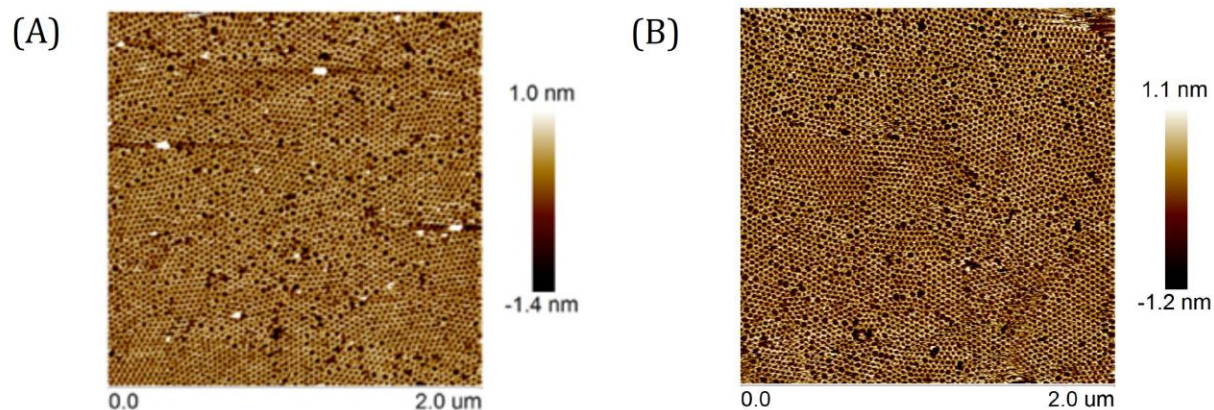
Figure 2-6 Atomic force microscopy (AFM) images of DNA 2D arrays on lipid bilayer with increased magnification. Anchor strands 30nt long.

We finally tested out approach in a real cell membrane system. Following the same protocol as lipid bilayer, cholesterol labeled DNA single strands are mixed with Hela cell in medium. The triskelion mimic DNA 3arm motifs are formed during cooling from 95° C to 60 ° C in TAE/Mg buffer. Then the sample was quickly cooling down to 37 ° C in about2 mins. During this short time, large array won't form. When these individual tiles mixed with anchor strand modified cells, the anchor strand will bind with individual single motif, bring them to membrane surface. Here, we chose the 20nt length anchor strand because it can form rigid hexagonal array in a lower concentration, and at the same time, can provide enough space for the array to tolerate the biomolecular on cell membrane. To characterize the array formation, we used a cy5 florescence dye labeled linker strand. If no array formed, the signal of single dye molecular will be too weak to be detected by florescence microscope. It is only visible when the hexagonal array is formed, which means the large amount of dye molecule with the linker strand are embedded in the arrays and generate a uniform fluorescence signal (Figure 2-7A). To exclude the possible reason that the aggregate of dye molecule will also generate the signal, a control experiment using anchor strand with linker strand complimentary sequence is performed. The dye molecules aggregated under this

condition and the resulted sharp dots signal was different from the array condition, as indicated in Figure 2-7B.
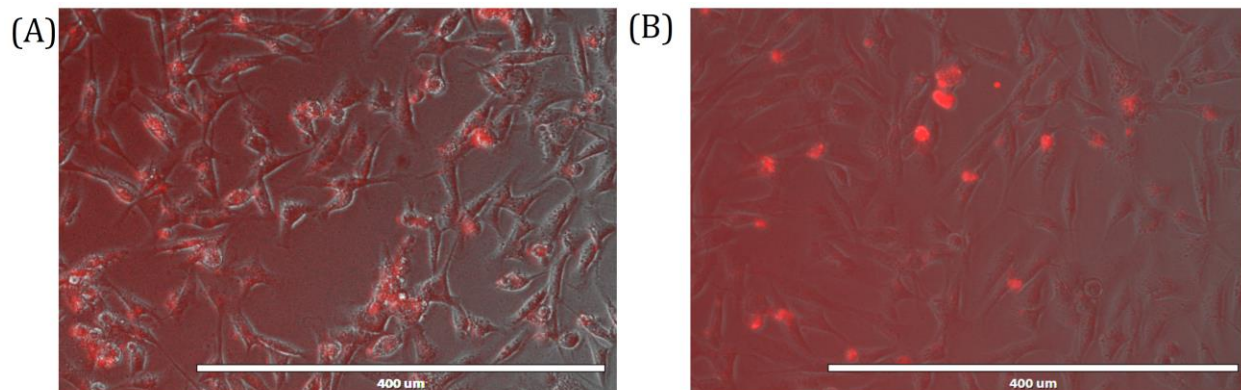
Figure 2-7 (A) Fluorescence image of clathrin patch mimicking DNA 2D arrays on cell surface (scale bar 400 um). (B) Fluorescence image of cy5 label single DNA strands mixed with cell. The sharp dots indicate the aggregate of dye (scale bar 400 um).

2.3   Conclusion

In conclusion, we successfully mimicked the clathrin patch formation using DNA 3arm motifs. In this study we explored clathrin patch mimicking using DNA single motifs on lipid bilayer membranes and on real cell surface. We found that DNA structures could be useful tools to mimic such biologic events. Furthermore, this lipid bilayer mediated DNA self-assembly not only can generate well-controlled nanopatterns on its surface, this large area regular patterns can also benefit many other fields. The short DNA strands used in this approach could be easily functionalized with other nanoparticles, including gold nanoparticles and quantum dots. And when those agents are organized in a micrometer pattern with nanometer scale defined geometry, they could exhibit many novel optical and electronic properties.

2.4   Methods

DNA Purification: Crude DNA of desired sequences were purchased from IDT (Integrated Device Technology, San Jose, CA). The DNA was purified by running a denaturing 20% polyacrylamide gel electrophoresis (PAGE) in TBE buffer (89mM Tris base, 89mM Boric acide, 2mM EDTA) at 55℃ at 600V. Purity of the purified samples was checked also by running PAGE.

Formation of the array: The array for gel assessment was achieved by annealing the mixture solution with molar ratio of lipo-1:lipo-2:lipo-3 being 1:3:3 in 1x TAE-Mg2+ buffer (89mM Tris base, 89mM Acetic acid, 2mM EDTA, 10 mM Magnesium acetate), and cooling it as following: 90˚C /5 min., 65˚C/30 min., 50˚C/30 min., 37˚C/30 min., and hold for 22˚C. AFM samples were prepared on a lipid coated mica surface. 10μL of 10mM of egg PC (L-α-phosphatidylcholine, Avanti Polar Lipids, Inc., Alabaster, AL) suspension were deposited on a 9mm diameter fresh cleaved mica. The solution sat on the surface for 2 minutes and was then blown off by compressed air. 50μL f 1μM cholesterol modified anchor strand was then deposited on the surface and incubated under 50 ˚C for 2 hours. The solution on the surface was blown off, and the mixture solution with molar ratio of lipo-1:lipo-2:lipo-3 being 1:3:3 in TAE-Mg2+ buffer with a expected final motif concentration of 0.1μM was deposited on the surface. The mica with solution was then annealed at 50 ˚C for 3 hours.

Native Polyacrylamide Gel Electrophoresis: The conjunction of the ssDNAs by hybridization was characterized by running a native 6% PAGE in in TAE-Mg2+ buffer at 100V in room temperature. Lane 6 of Figure 2-3 shows that the stoichiometry was accurate leaving the product stuck in the well and little of the component material get into the gel.

AFM Imaging: AFM imaging was performed under room temperature in a fluid chamber to avoid disruption of the structure. The sample was imaged in 1×TAE-Mg2+ buffer. SNL-10 tip (Bruker, Camarillo, CA) with a spring constant of 0.24N/m was used on a Multimode AFM (Vecco Metrology, Santa Barbara, CA). Amplitude setpoint was controlled at the lowest possible value to avoid scratching on the structure.

***In Vitro* Formation of Arrays:** Approximately, 7×103 cells were seeded in a well containing Corning cellar DMEM media with 4.5 g/L glucose, L- glutamine, and sodium pyruvate; 10% Hylcone Bovine Growth Serum (FBS); and 1% penicillin streptomycin, and incubated at 37 °C for 24 h. 50μL f 1μM cholesterol modified anchor strand was then added and incubated under 37 °C for 30 mins. The mixture solution with molar ratio of lipo-1:lipo-2:lipo-3 being 1:3:3 in TAE-Mg2+ buffer with an expected final motif concentration of 0.1μM was added. The result was imaged using an EVOS fluorescent cell imaging system after a 2-hour incubation. All the experiments were carried out at room temperature.

Chapter 2, in part, is in preparation for publication with coauthor Y. Chen. The dissertation author is the first author of this work.

CHAPTER 3: 2D-3D Transition of DNA Nanostructures

3.1 Introduction

Dynamic structure conformation change has played a crucial role in many biologic processes. For example, the cell uptake of foreign objects through clathrin-mediated endocytosis depends on the clathrin patch bending to form polyhedron vehicles[27,28]. DNA nanotechnology has enabled fabrication of a diverse range of sophisticated structures, including two-dimensional DNA arrays[29,30], and three-dimensional DNA nanoobjects[31,32] and DNA nanomachines[33–41]. Among these, dynamic DNA nanostructures shows a promising ability in nanometer scale control. Many approaches have been developed, including strand displacement[33–36], DNA enzyme[37,38], and reconfiguration of arrays from different DNA motifs[39–41]. These devices can sense a range of physical or chemical cues. However, these existing devices can only adopt simple dynamic behaviors that happened in a single unit and in a small range change. The different dimensional transformation is missing.

Here we demonstrated a 2D-3D transformable DNA nanostructure. We showed that by fueling the DNA nanostructure with DNA strands, they can perform a cross-dimensional switch, which simulate some of the key aspects of biological processes, such as triskelion protein bending in clathrin patch formation. We further showed that the DNA array can possibly accumulate the curvature or energy in each individual unit conformation change to the extent that it could breakdown lipid bilayer, which simulate the cell membrane engulf.

3.2   Results and Discussion

Design of transformable DNA nanostructures: We used short DNA strands as building block to construct the DNA nanostructures. As showing in Figure 3-1a, a DNA point-star motif is used. It consists of one center strand, three arm strands and three end strands with two linker strands on each. The linker strands can partially hybridize with the others linker strands on another end strand, and left a single strand with hairpin domain. A single block strand can hybridize with these single strand domains to form rigid double strand domain. The overall transformation is controlled by this linker strand. When there is block strand, the extended double strand domain is formed with length 12.2 nm. When a DNA fuel strand is introduced, it is fully complementary with the block strand. It will then hybridize with the block strand and extract it from the DNA nanostructures, with single strand domain remaining. This single strand will then form a hairpin structure. The overall length will decrease to 6.5 nm (Figure 3-2). Because the linker strand controls the arm distance, to overcome the tension, the DNA nanostructure will then bend, switch from a flat form to a convex form (Figure 3-1b).
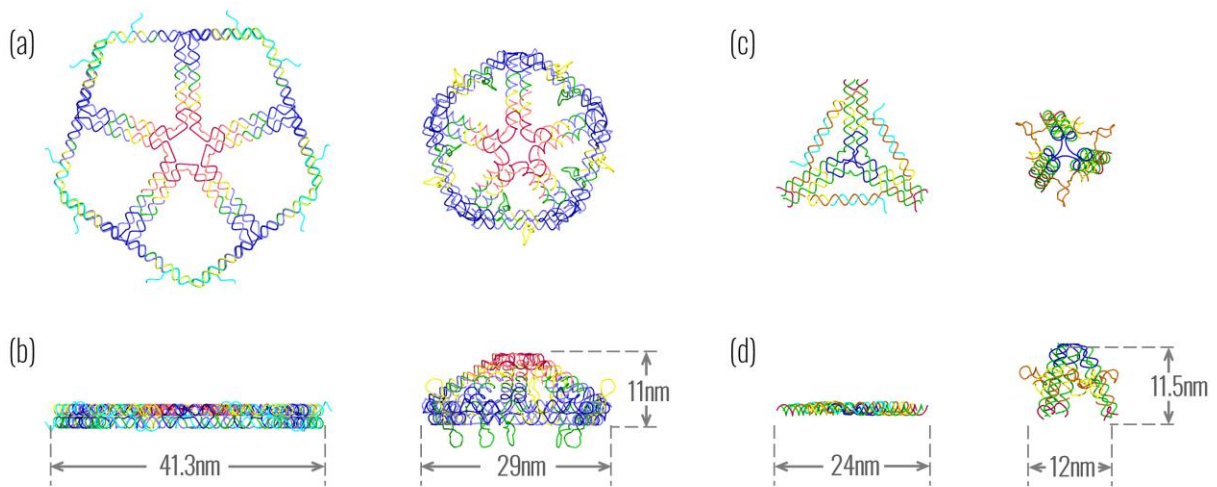
Figure 3-1 Illustration and dimensions of 5-arm single motifs (a,b) and 3-arm array motifs (c,d). (a): Top-down view of 5-arm 2D (left) and 3D (right) motifs. (b): Side view of 5-arm 2D and 3D motifs. (c): Top-down view of 3-arm array 2D (left) and 3D (right) motifs. (d): Side view of 3-arm array 2D and 3D motifs.
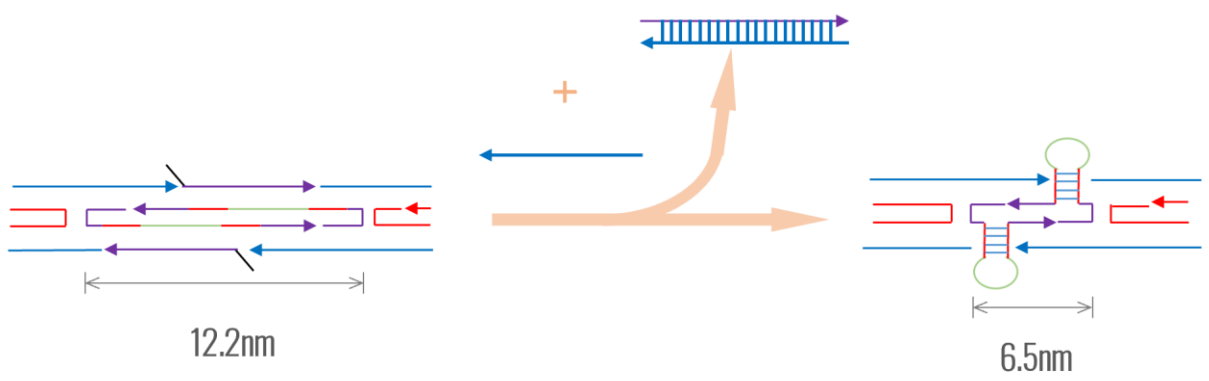
Figure 3-2 Demonstration of fuel-strand mediated transformation process in single motifs. The fuel strand takes away the extension strand, and the single-stranded domain that is left behind is deigned to form a hairpin structure, shortening the overall length of the linker.

One-pot assembly of DNA nanostructures: The transformation of DNA nanostructures is expected to be dictated by the DNA fuel strands. To investigate the two stable states, we first studied the 2D and 3D structures with 5-arm design. We choose this design because 5-arm are more stable than 3-arm with more linker strands domains. Native gel electrophoresis of the 5-arm in 2D formation and 3D formation is overserved in Figure 3-3c Lane1 and Lane 2.

In the same gel we tested the transformation process mediated by DNA fuel strand. We started with 2D flat form. After adding fuel strand, the DNA nanostructure lost the extension strand. The single strand domain left behind will then form the hairpin structure on the linker strand and force the flat form to switch to a convex form. As the molecular weight becomes smaller, so does the size of the cross-section. The structure thus will migrate faster in native gel electrophoresis (Figure 3-3c. Lane 1). To conform the result, we add extra fuel strands to exclude the possibility of random hybridization from happening (Figure 3-3c, Lane 5 and Lane 6). We then perform the transformation from 3D to 2D as well, and show a similar but reversed pattern (Figure 3-3c, Lane 3,4).

Transformation of single DNA unit with 5 arms: To directly monitor the transformation result, we performed the AFM measurement. Figure 3-3b left showed the 3D form of DNA nanostructures. Each nanostructure is 12 nm in diameter, while the 2D form in the middle panel showing each individual unit switched to 25 nm. This observation was further confirmed through DLS measurement (Figure 3-3d). The hydro-dynamic size of the 5-arm motif in compact 3D form is around 25 nm. The flat 2D form is around 50 nm. This is because the flat form DNA nanostructures can't be precisely measured under DLS because of its shape factor, compared with the 3D form which is closer to a sphere.

Figure 3-3 5-arm single motifs 2D<->3D transitions illustrations and characterizations. (a): Demonstration of 2D to 3D and back to 2D transitions. From left to middle: addition of Ex strands makes the hairpin strand expand into a double helix, in turn expanding the distance between the distance between the central 5-arm vertices. This makes the 3D structure flatten into a 2D structure. From middle to right: addition of the Fu strand extracts the Ex strands in the structure, turning the 2D structure back to 3D structure. (b): AFM images of respective steps in (a) confirming the formation of the two structures. (c): 5% native PAGE gel in TAEMg2+for the formation and transformation of single 3D and 2D motifs. Lane 1: 3D structure; Lane 2: 3D structure with 1:1 molar ratio of Ex strand added; Lane 3: 3D structure with 1:3 molar ratio of Ex strand added; Lane 4: 2D structure; Lane 5: 2D structure with 1:3 molar ratio of Fu strand added; Lane 6: 2D structure with 1:3 molar ratio of Fu strand added before anneal. Upper bands indicate the flat 2D structure, because of its rigidity. Lower bands at ~1k bp indicate 3D structure, because of its relatively compact structure. (d): DLS measurements for 5arm-2D and 5arm-3D. A shift from ~20nm to ~70nm of the major peak was observed, indicating that the structure underwent transformation of shape and/or size.

(a)

(b)

(c)

(d)
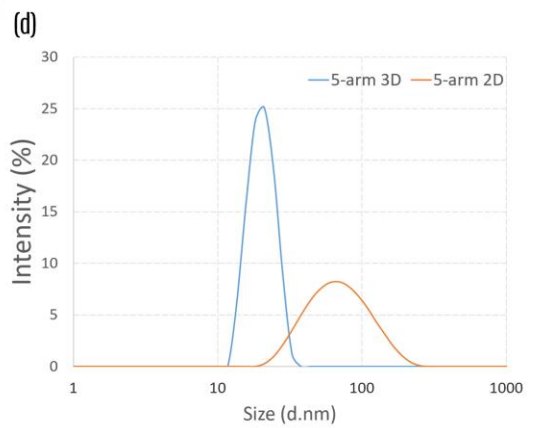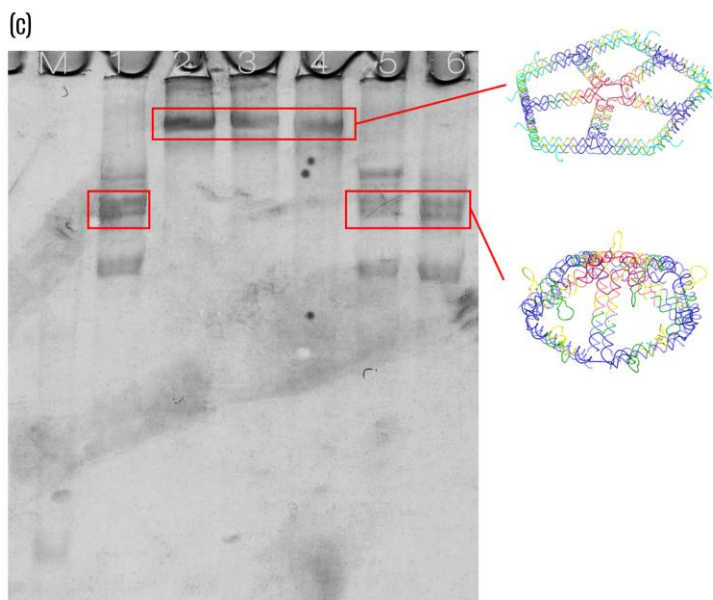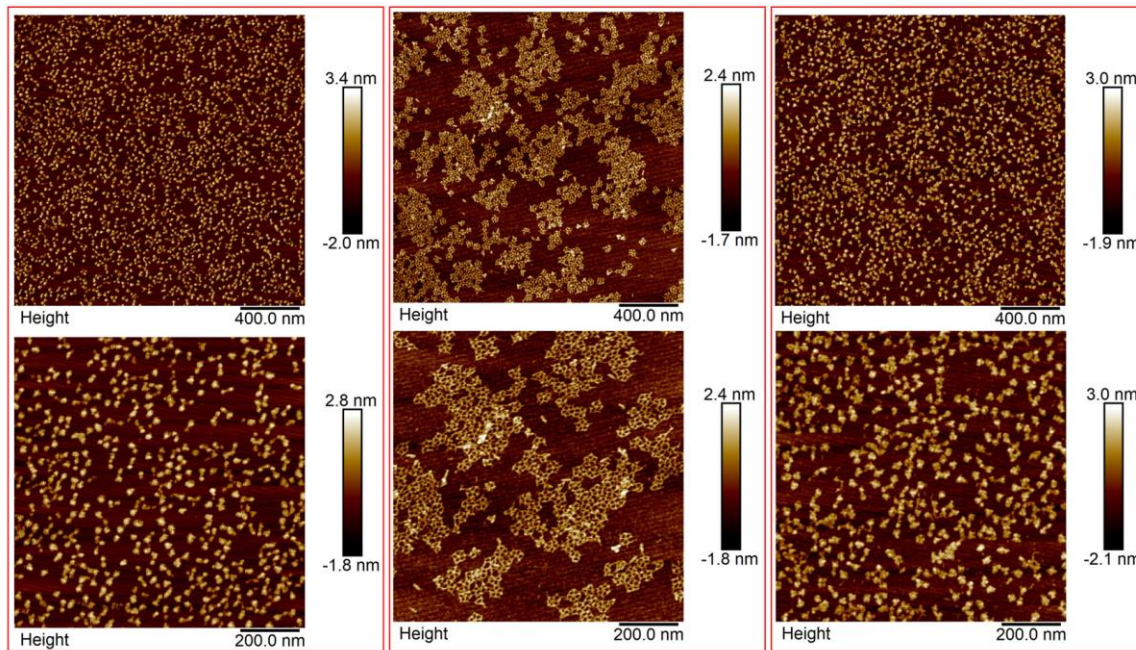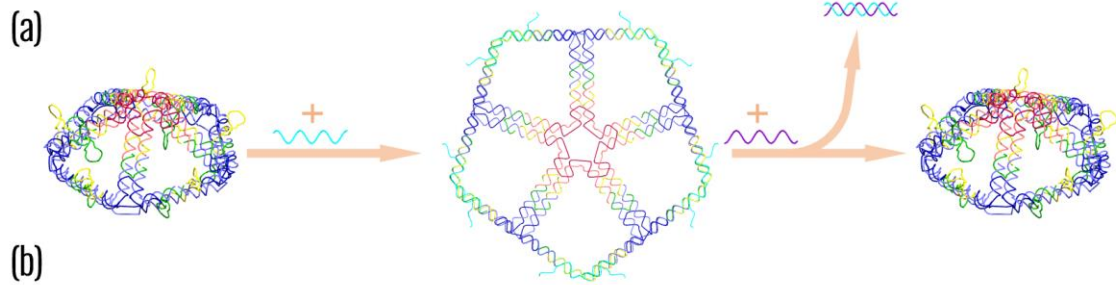
Transformation of single DNA unit with 3, 4, 6 arms: Similar design and characterization were done for 3, 4, 6 arms motifs as well. A variation in numbers of arms gives the system flexibility in terms of tuning the heights and angles of the resulting 3D structures. The predicted change in height and angles for different arm numbers are shown in Figure 3-4. Interestingly, under AFM, we found out that the difference between the 3D and 2D states is more prominent in 5-arm and 6-arm than 3 and 4. This can be seen by comparing the 2 states of different arm designs in Figure Y. In order to find out the cause for this difference, we conducted molecular dynamics simulation on the structure. The simulation work was predominately contributed by Xiangyi Dong. From the simulation images of the structure in Figure Z, we can see that the 3-arm structure is strained and is not completely flat in the 2D state. When transformed to the 3D state, the change of angle is so sharp that the shape is actually similar to what it was in the supposed 2D state. This explained why the AFM of 3-arm 2D and 3D states looked similar. Contrarily, for the 5-arm motif, its 2D motif can actually stretch and expand to a flat structure, and the 3D state is visibly more compact. This matches what we see in the AFM images. The sizes also match the simulation results and the AFM images. For the 2D to 3D transition, the circumradius in AFM changed from 12.9 nm to 11.9nm and for the simulation results from 11.9 nm to 9.9nm. For the 2D 5-arm motif, the area of the motif is 1498 nm^2 in AFM vs. 1556 nm^2 in simulation results. This simulation result indicates that the linker length is not optimized for the 3-arm and 4-arm structures. It was likely the strain caused by the double cross-over that was not taken into consideration, that ultimately caused the shorter-than-expected linker domain length. To optimize the structure, the linker length needs to be reassessed. Nonetheless, the goal for this part of experiment was achieved, that is designing a reversible transformation mechanism with DNA

nanostructures. In the next section, we combined this mechanism with the DNA array formed on a lipid membrane, that is similar to the structure in Chapter 1.
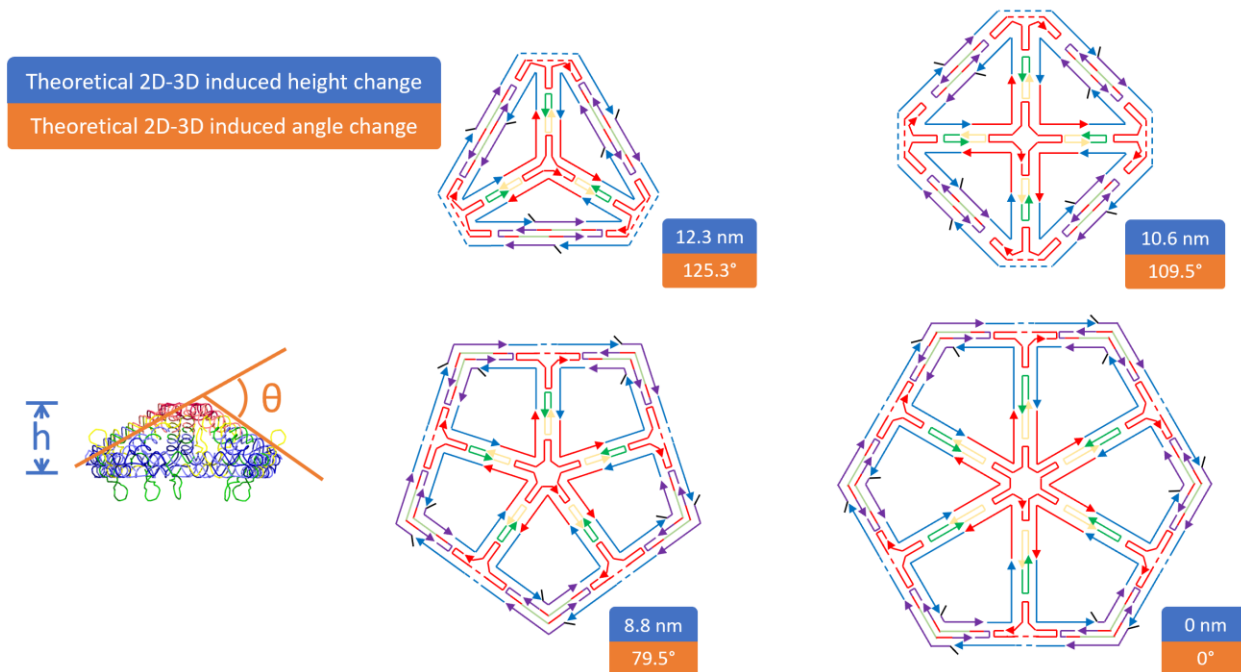
Figure 3-4 Designs of 3-arm, 4-arm, 5-arm, 6-arm motifs and their respective theoretical 2D-3D induced height and angle changes.
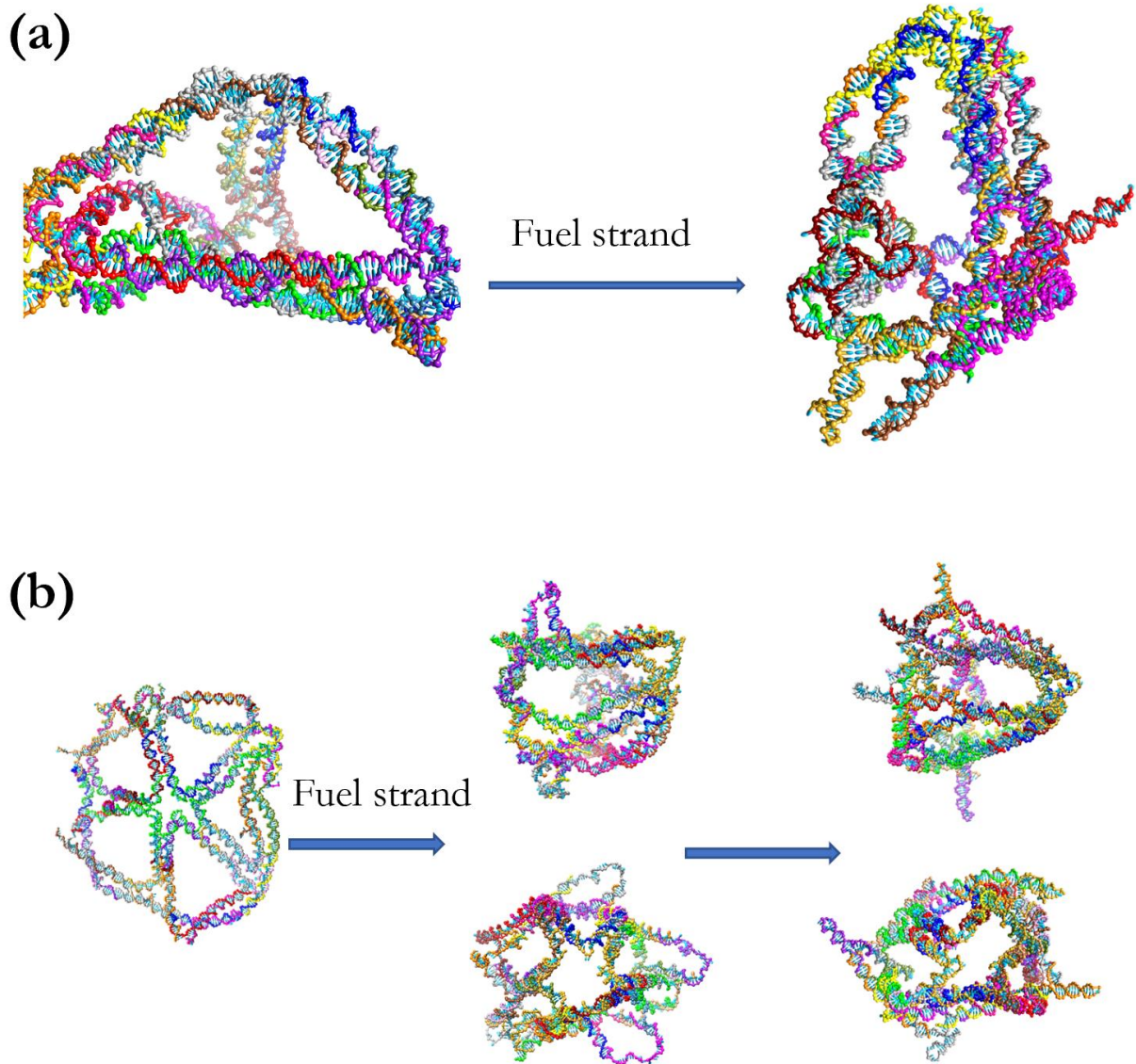
Figure 3-5 Simulation results of the shape of 3-arm and 5-arm motifs. (a): 3-arm motif transformation from 2D to 3D. (b): 5-arm motif transformation from 2D to intermediate state to 3D.

Figure 3-6 (a,b,c): Mechanism of transition and 3D demonstration of 2D to 3D transition (a): The angle between two arms was 120° when the motif is in 2D configuration. Once Fu strand is added, it binds to the overhang on the side bridge connecting the two arms, ripping of the strand off the structure and forms a double helix by itself. (b) The bridge strand was designed so that it can form a hairpin structure when not in a hybridized condition. The result of the formation of the hairpin is that the bridge section was shortened from 12.2nm to 6.5nm, bringing two arms closer together. (c) Once the two arms were brought closer by the shortened bridge section, the angle was reduced to 46.2°. Because all three angles undergo the same change, with the flexibility induced by loop structure in the central strand, the structure was forced to deform in the z direction, resulting in the structure "standing up" and becoming a pyramid-like structure. (d): 5% native PAGE gel in TAEMg^{2+} for the formation and transformation of array-forming 2D and 3D particles. The samples were made according to the ratio for each lane. They were incubated in a PCR cycler, slowly cooled down from 90°C to room temperature. Lane 1: 2D structure; Lane 2: Lane 1 + 3x molar amount of Fu strand and incubate for 2 hrs; Lane 3: Lane 2 + 3x molar amount of HB strand and incubate for 2 hrs. Lane 4: 3D structure; Lane 5: Lane 4 + 3x molar amount of HB strand and incubate for 2 hrs; Lane 6: Lane 5 + 3x molar amount of Fu strand and incubate for 2 hrs. All transition incubation were under 37°C. (e): In-air AFM images of array-3D and array-2D single motifs. Left: 3D single motifs. Size of each particle is about 10nm. Middle: 2D single motifs after transition. Size of each particle is about 20nm. 3-arm structures can be clearly observed from these AFM images. Right: 3D single motifs were achieved from transition from 2D motifs, completing one transition cycle.

(b)

12.2nm

6.5nm

θ = 120°   θ = 120°   θ = 46.2°

(a)   (c)

(b)

12.2nm

6.5nm

(a)   (c)

(d)

M 1 2 3 4 5 6

(e)

Height   100.0 nm   Height   100.0 nm   Height   200.0 nm

2.2 nm   2.3 nm   2.4 nm

-1.7 nm   -1.9 nm   -1.6 nm
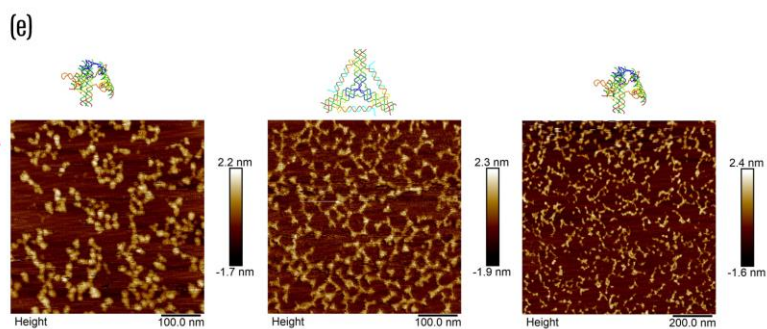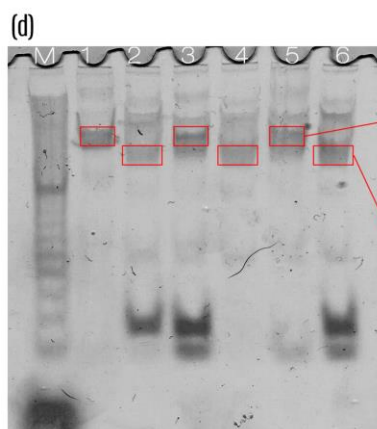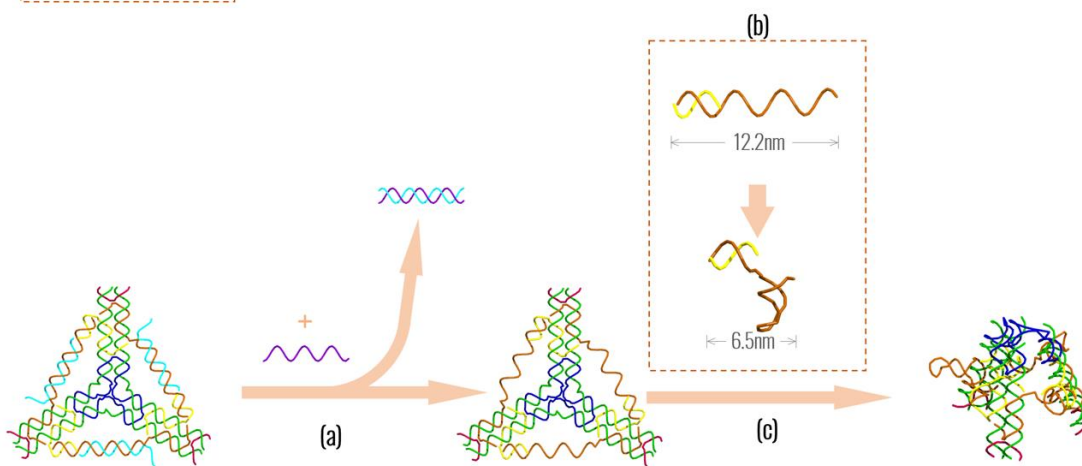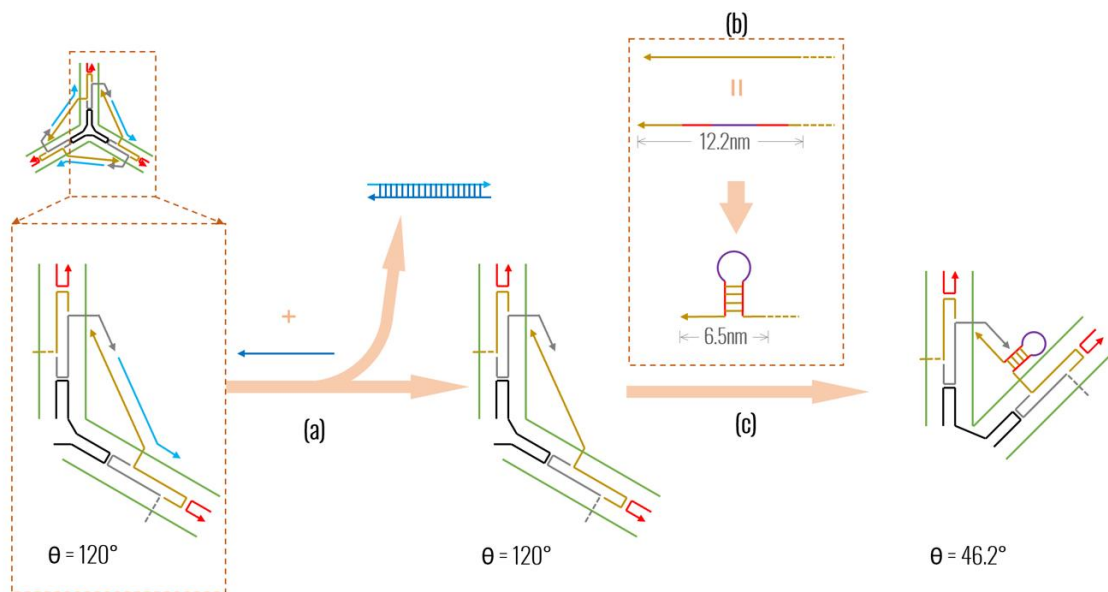
Transformation of DNA arrays: One advantage of this platform is the structure conformation change can be accumulated. DNA three arm design was proven to be successfully to construct DNA arrays. First, we tested the stability of individual 3 arm motifs. Native gel electrophoresis showed this motif can perform multiple cycles switching between 2D flatform and 3D convex form (Figure 3-6d). AFM images also showed reversible morphology changes (Figure 3-6e).

We then tested out this platform in a simplified version of a cell membrane system, i.e., a supported lipid bilayer on mica. Following tradition lipid bilayer formation, Egg pc lipids molecular are coated on a mica surface. Then, the cholesterol labeled DNA single strands are mixed with lipid bilayer in buffer. Due to its hydrophobicity, the cholesterol will insert into bilayer and bring the linked DNA strands attached to lipid bilayer surface. The DNA 3-arm motifs are formed by cooling from 95°C to 60°C. At this temperature, the units could not stably associate with each other but instead remained as individual motifs and strong enough to hybridize anchor strand. When these individual motifs mixed with anchored lipid bilayer, the anchor strand will bind with individual single motif, bring them to membrane surface. Once these motifs are recuited onto the lipid surface, the sticky ends at each individual motif can start to self-assembly when temperature decrease. Due to the fluidity of lipid membrane, the anchor strand with cholesterol could move freely on it and facilitate the association of individual motifs and make them self-assemble into desired patterns.

After assembly on lipid bilayer surfaces, the DNA nanopatterns were examined directly by AFM (Figure 3-7c). Hexagonal patterns are clearly visible. Such patterns are consistent with the molecular designs and are essentially the same as the patterns observed as clathrin patch. In the hexagonal array, the size of the edge is around 15 nm, which is comparable with the real clathrin

40

patch. After adding the fuel strands, we observed that with the accumulation of each individual unit conformation change, the lipid bilayer is broken.

Although theoretically, the sum of zipping force from the hairpin formations is about 33 pN[42]. It is almost 700 times smaller than the puncture force for the membrane in the literature[43]. We suspect that the breakdown of the membrane was cause by the accumulation of the curvature change throughout the whole array network, since the force from the conformational change from individual motif is much too small to break the membrane.
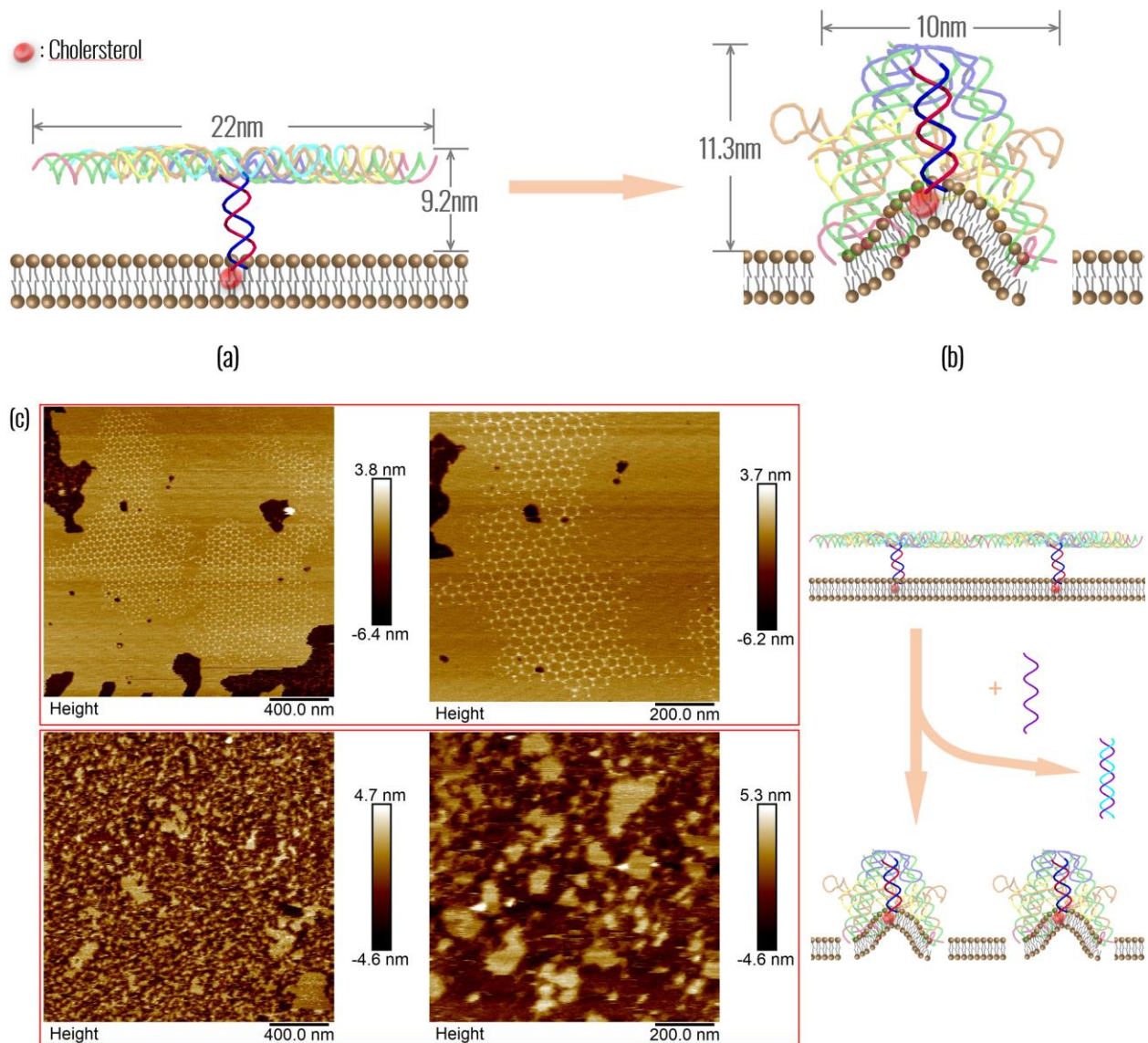
Figure 3-7 (a,b) Demonstration of lipid-breaking mechanism of the 3-arm array system on a mica-supported lipid bilayer. (a): 3-arm motif are connected to each other by base stacking interactions. The overhang from the central strand binds to a complimentary strand with one end connected to a cholesterol molecule, that is stuck in the lipid bilayer. (b): after adding the FU strands, the structure changes and tends to drag the cholesterol molecule out, deforming the lipid bilayer. Due to hydrophobic interaction between the tips of the 3D structure and the hydrophobic layer in the center of the lipid bilayer, the bilayer was broken into pieces. (c): In-liquid AFM images of array-2D arrays on lipid and array-3D after transition. Top: Hexagonal arrays can be seen forming on the supported lipid bilayer. The size of each unit is about 20nm in diameter. Bottom: Broken pieces of supported lipid bilayer after the transition happens. The array shrank into small 3D pyramid-like particles and the lipid layer was forced into small pieces in the process

3.3 Conclusion

Our work has demonstrated a general strategy for the construction of transformable DNA nanostructures. A flatform nano-object can transfer to a convex form nano-object. Furthermore, the accumulation of each individual unit transformation can accumulate. Through the study of these DNA arrays, we have demonstrated controlled, multistep, long-range transformation of the DNA arrays. This dynamic behavior can be regulated by the shapes and sizes of arrays and by external factors.

We expect that our new DNA dynamic arrays will provide clues on how to construct nanostructures with dimensional dynamic behaviors, and may enable a range of applications using dynamic DNA arrays. For example, the dramatic curvature change in the DNA nanostructure array resembles crucial features of cell membrane engulf that are observed in biological systems. Therefore, our artificial arrays may serve as model structures to investigate and validate underlying mechanisms of cell entry, or be used to design and construct delivery metamaterials. The DNA arrays may also be used as a platform to analyze biomolecular interactions at a single-molecule level, by controlling the single molecular interactions to conformational changes in the DNA nanostructures. The ability to construct dynamic DNA structures with controlled, dimensional change should improve the sophistication and functionality of such hybrid functional structures.

3.4 Materials and Methods

Purification of DNA: Sequence were sent to IDT (Integrated Device Technology, San Jose, CA) to manufacture crude strands. They were further purified by a denaturing 20% polyacrylamide gel electrophoresis (PAGE) in TBE buffer (89mM Tris base, 89mM Boric acid, 2mM EDTA), 55℃, 600V. The purity of each strand used was verified by another denaturing PAGE gel under same conditions.

Formation of DNA 3-arm motifs: Under native conditions, the buffer used is 1x TAE-Mg2+ buffer (89mM Tris base, 89mM Acetic acid, 2mM EDTA, 10 mM Magnesium acetate), unless specified otherwise. The DNA strands that form the individual 3-arm motifs were mixed in the molar ratio of 1:3:3:3:3:3 for strands L3:M:S:J1:J2:HB in native condition. The solution was then taken to a PCR cycler, heated up to 90˚C for 5 mins, and then slowly cooled down to room temperature. The annealing process was programmed as: 90˚C /5 min, then 85˚C to 10˚C in 0.1˚C interval every 2 mins. The resulting motif and pre-array were verified by running a 5% native PAGE gel.

Native Polyacrylamide Gel Electrophoresis: The single strand DNA that consist the motif are combine in different ways in order to verify the exact formation of the motifs. The different combinations were characterized by running a native 5% PAGE in in TAE-Mg2+ buffer at 150V in room temperature for 60 mins. The formation of the motifs can be confirmed by native gel. Lane Y indicates that while fuel strands (Fu) are present, different structures form and those could potentially be the 3D particles that were expected. Another 5% native PAGE gel was run to test the reversibility of the reaction. The 2D motifs were formed first and a portion of it was preserved for gel running. Then 3x molar amount of Fu strands were added. The sample was then incubated for 1 hr at room temperature. A portion of the resulting solution was preserved for another lane of the gel. 3x molar amount of HB strand were added after that and the solution was incubated for another hr under room temperature. This procedure was done in the same fashion with a starting structure of 3D motifs.

Formation of hexagonal DNA arrays on supported lipid bilayer on a mica surface: Egg PC (L-α-phosphatidylcholine, Avanti Polar Lipids, Inc., Alabaster, AL) and cholesterol in a molar ratio of 9:1 was dissolved in chloroform and dried, then hydrolyzed using 1x TAE-Mg2+

¬solution to make a 10mM solution of lipid vesicles. The solution was extruded using a 400nm size filter, in order to obtain uniform single-layered vesicles. 10μL of the extruded solution was deposited on a freshly cleave mica surface, and let sit for 10 mins. 5uL of pre-made 4μM 20T-cholersterol was deposited on the mix afterwards and let sit for 30 mins. The solution was then blown away using compressed air, and a total amount of 20 nmol DNA 3-arm motif solution was added to the surface and let sit for 2 hrs. The amount of DNA motifs is determined so that the array formed would cover 150% of the mica surface area. The sample was then characterized by AFM.

Transition of DNA arrays into 3D particles: Another identical array-on-lipid was prepared for the experimental group of transition using the procedure described above. 3x molar amount of Fu strands were added to the solution. The solution was incubated in a 37˚C oven for one hr. Extra caution was taken to avoid the drying of the solution on the mica. This sample was also characterized by AFM.

AFM Imaging: Tapping mode in liquid is used for AFM imaging for the DNA structures. The sample was imaged in 1×TAE-Mg2+ buffer. SNL-10 tip (Bruker, Camarillo, CA) with a spring constant of 0.24N/m was used on a Multimode AFM (Vecco Metrology, Santa Barbara, CA). Amplitude setpoint was controlled at the lowest possible value to avoid scratching on the structure.

DNA simulation: To look deep into the structures and study the morphology, we applied DNA simulation by oxDNA, a coarse-grained model which provide the possibility of molecular-scale observation. Previously, oxDNA has shown an excellent representation of DNA structure, including DNA three-dimensional structures, DNA origami, toe-hold mediated strand placement (TMSD). We implement the MD simulation of our TMSD triggered conformation change to our design. The MD simulations were performed at room temperature (298 K) with a monovalent salt

concentration of 0.5 M Na$^+$. The high salt concentration was widely used for DNA structure

simulation to screen repulsive interactions. Because our design highly depended on the sequence,

we used the sequence-dependent DNA interaction. Each structure was run at least 106 steps to

reach a more realistic state.

DNA strand sequences used in this chapter:

3-arm central strand:
5'-AGGCACCATCGTAGGTTTCTTGCCAGGCACCATCGTAGGTTTCTTGCCA
GGCACCATCGTAGGTTTCTTGCC-3'

4-arm central strand:
5'-
AGGCACCATCGTAGGTTTCTTGCCAGGCACCATCGTAGGTTTCTTGCCAGGCACCAT
CGTAGGTTTCTTGCCA GGCACCATCGTAGGTTTCTTGC-3'
CTTGCCAGGCACCATCGTAGGTTT

5-arm central strand:
5'-
AGGCACCATCGTAGGTTTCTTGCCAGGCACCATCGTAGGTTTCTTGCCAGGCACCAT
CGTAGGTTTCTTGCCAGGCACCATCGTAGGTTTCTTGCCA
GGCACCATCGTAGGTTTCTTGC-3'

6-arm central strand:
5'-
AGGCACCATCGTAGGTTTCTTGCCAGGCACCATCGTAGGTTTCTTGCCAGGCACCAT
CGTAGGTTTCTTGCCAGGCACCATCGTAGGTTTCTTGCCAGGCACCATCGTAGGTTTC
TTGCCA GGCACCATCGTAGGTTTCTTGC-3'

RM:
5'-TAGTGTCATGCCTGGCAAGCCTACGATGGACAGAGTGCGTGG-3'

RSY:
5'-CACTCTGT TGACACTA CATGC-3'

BSG:
5'-ATCCGACT CGAGCGAG CCACG -3'

BL1:
5'-GTACA CCAGTGAAGT TTTTT CGTTGCGATCA CCAACGGAGT TTTTT CGATCC
TAGCA CCTCTGGAGT TTTTT TCTGCC-3'

BM1:
5'-CTCGCTCG TGATCGCAACG ACTTCACTGG ACACGGTAACGCC-3'

BM2:
5'-TAGCAACC TGTACGGCAGA ACTCCAGAGG AACCACAGAGCAT-3'

BM3:
5'- ACCGCACG TGCTAGGATCG ACTCCGTTGG AGTCGGAT GCATG-3'

BH1:
5'- CGTGTGGTTGCTA AAA GAG AAC CTC TAG ACT AAG GTT CTC TTT ATGCTCTG -3'

BH2:
5'- TGG TTC GTG CGG TTC TTG GAC AGA ATG GTT ACA GTG TCC AAG AGG CGT TAC -3'

EX1:
5'- CTC CTG TAT CTT GGA CAC TGT AAC CAT TCT GTC CAA GA -3'

EX2:
5'- ACG CAA TGA AAG AGA ACC ATA GTC TAG ACG TTC TCT TT -3'

FU1:
5'- TCT TGG AGA CAA TGG TTA CAG TGT CCA AGA TAC AGG AG -3'

FU2:
5'- AAA GAG AAC GTC TAG ACT ATG GTT CTC TTT CAT TGC GT -3'

L3:
5'- AGGCACCATCGTAGGTTTCTTGCCAGGCACCATCGTAGGTTTCTTGCCAGGCACCAT CGTAGGTTTCTTGC-3'

M:
5'- GCAACCTGATACCCTTAGTATGTAGCCTGCCTGGCAAGCCTACGATGGACAATCTAT TATGCGATTCGGACACGG-3'

S:
5'-CCGTGTGGTTGC-3'

J1:

5'-
TATCACCGAATCGCATAATACCACCTGTGTCATTGGTAACACAGGTTGCGGTGGCG -
3'

J2:
5'- ATTGTGGCTACATACTAAGGGCCGCCACCGCA -3'

HB:
5'- ACCTGTGTTACCAATGACACAGGTGTCCAAGA -3'

Fu:
5'- TCTTGGACACCTGTGTCATTGGTAACACAGGT -3'

Chapter 3, in part, is in preparation for publication with coauthors M. Kai, X. Dong, Y. Chen. The dissertation author is the joint first author of this work. The dissertation author is the first author of this work.

CHAPTER 4: DNA Nano-Delivery Systems

4.1   Introduction

4.1.1   Drug delivery and DNA nanostructures

Naked therapeutic agents, which include small-molecule and bio-molecular drugs, have some intrinsic issues that prevent the full realization of their functions in the body. This includes poor solubility, poor stability against chemical and enzymatic degradation, inability to pass the biologic barriers, unwanted side effects and toxicity. To overcome these challenges, many different drug delivery systems have been developed in the past decades[44,45]. They can be classified into two categories: natural vector systems, such as virus[46] and red blood cells[47], and synthetic drug carrier systems, the majority of which are comprised of liposomes and polymer particles[48,49]. These cargos use natural or synthetic particles to capture drugs to bypass their physiochemical limitation and barriers to effective delivery. Through appropriate parameter design, these delivery systems effectively increase the drug loading efficacy, the circulation time in body, and the final therapeutic results[50,51]. Many of them have been proved for clinical use or clinical trials.

Although these drug carriers are being actively developed, there is still a measurable gap that has to be surmounted to achieve the ultimate goal of drug delivery: the maximal therapeutic efficacy with minimal toxic effects. In spite of different rout of administration, oral, injection, transdermal or inhalation, all delivery systems can be traced to the cellular level. This stimulates the exponential development of nanomedicine which uses the nanotechnology tools for better drug targeting and less toxic therapeutic effects, as well as diagnostic properties[52,53]. Among all of these newly developed delivery systems, DNA nanostructures show high promise. DNA is a biopolymer that can self-assemble into double helices through by Watson–Crick base pairing and is stabilized by hydrogen bonds, p–p stacking, and hydrophobic interactions. They have well-defined

structures: the helical turn is 3.4 nm and the diameter is ~ 2.2 nm for the B-form double-helical molecules. Fueled by this base-pairing ability, DNA nanotechnology developed many strategies to form DNA nanostructures with well-controlled size, shape, and surface chemistry. In nanomedicine, these properties strongly affect the delivery capacities[54,55] and thus give DNA nanostructures a unique control ability to address some of the delivery challenges.

4.1.2 Delivery process

There are many methods that have been coupled to DNA nanotechnology to effectively deliver therapeutic modalities. It includes drug modalities, gene-silencing modalities, and the incorporation of cellular targeting into DNA nanostructures. Many DNA drug delivery systems include the incorporation of doxorubicin (Dox), an anti-cancer therapeutic[17,56], as the proof of concept for small molecular drug delivery. Dox can intercalate into the DNA structure and allow it to form properly by relieving torsional stress, as showed in Figure 4-1[56–58]. However, despite Doxs potency as an anti-cancer drug, it can have serious side effects when it accumulates off-target such as cardiomyopathy, which can lead to congestive heart failure[59]. Therefore, avoiding off-target or premature delivery must be achieved.
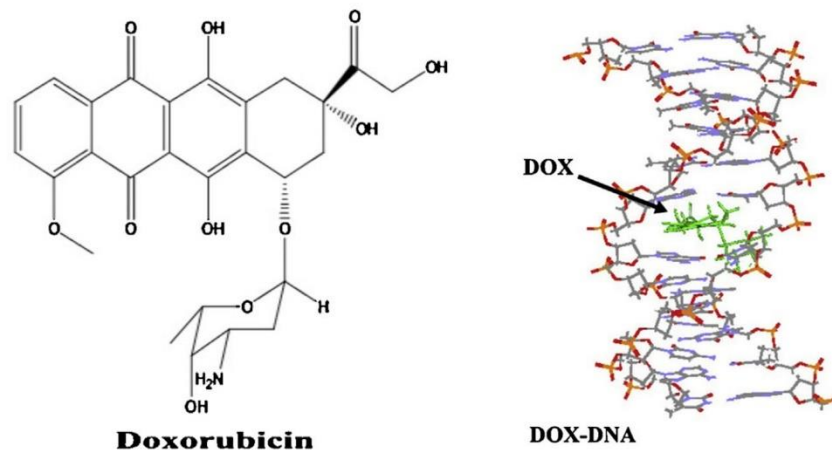
Figure 4-1 Intercalation of Doxorubicin[57]

Another popular therapeutic technique that many researchers have been taken advantage of is gene-silencing through RNA interference[60]. siRNA in particular has been utilized by many researchers for therapeutic gene silencing and can be modified to be target specific to avoid off target silencing effects[61]. RNA interference can usually be used without triggering the immune system, however introducing the artificial siRNA can monopolize the natural interference pathway of the RNA silencing complex, which is an important part of the cellular function[62]. One of the biggest challenges in RNA delivery is stability in vivo, but chemical modifications of the oligomers can increase the stability[63].

Targeting can be achieved through the use of DNA aptamer sequences and also through the use of functionalizing the DNA with targeting ligands and can help avoid many of the undesirable off target effects[59,64,65]. For example, Zhu *et al.* created synthetic DNA adducts to allow for targeted anti-cancer delivery. These take advantage of the overexpression of certain receptors during cancer[66].

Once been uptake by cells, DNA nanostructure can incorporate environmental triggers to release loaded drugs, such as linkers that are responsible to changes in the pH[56,58,67,68]. This technique can also aid in mapping the pH changes inside the cells itself, as reported by Modi *et al*[68].

There are several possible pathways for these DNA nanostructures to enter the cell and these can be explored by using inhibitors to block certain pathways[69,70]. These pathways can be divided into two types: endocytotic pathways and non-endocytotic pathways[71]. The endocytotic pathways include phagocytosis, clathrin mediated endocytosis, caveolae mediated endocytosis, and macropinocytosis. However, it is not well understood what mechanism is responsible for the successful uptake of DNA nanostructures. Preliminary data such as that demonstrated by Chen *et al.* suggested clathrin receptor mediated endocytosis[70]. They measured the mechanism of the uptake of their RCA nanoribbons through inhibitors such as chlorpromazine, a clathrin inhibitor, genistein, a caveolae mediated inhibitor, methyl-β-cyclodextrin, a lipid-raft endocytosis inhibitor, wortmannin, a macropinocytosis inhibitor, and NaN3, an energy dependent endocytosis inhibitor. Final results suggested that the uptake is clathrin mediated and lipid raft mediated endocytosis.

Chen *et al.* also studied the mechanism of transfection of DNA nanoparticle (DNPs) and suggested that nucleolin is a good target for non-viral gene delivery with the presence of glucocorticoid receptor (GCR)[72]. Disruption of a raft protein, flotillin also decrease the transfection of DNPs, while inhibition of other endocytic pathways barely affects the process.

The cell membrane carries a net negative charge and nucleic acids also carry a net negative charge[73]. As a result, Some DNA nanostructures, not containing targeting modalities, may need some kind of cationic transfection agent, such as Lipofectamine, to increase the cellular uptake and therapeutic efficacy[73]. Positively charged intercalators or positively charged proteins, such as

Dox, viral capsule proteins, or cationic polymers, may also help reduce the net negative charge thus reducing the electrostatic repulsion in the DNA structure itself and between the DNA nanotechnology and the cell membrane[60,74–76].

4.1.3 Delivery vehicles

Due to the precise and predictable pairing nature of DNA chains, size and shape of the nanoscale DNA constructs can be designed to fit the needs. Moreover, overhangs can be introduced on to the structures to allow easy functionalization of fluorescent dyes, targeting agents or even drugs.

The oligonucleotide strategy was reported first by Nadrian Seeman in 1983 and is widely considered the original basis of DNA nanotechnology. He synthesized a stable 4 arm junction with 4 sixteen base pair strands by minimizing the strand symmetry[2]. The oligonucleotide strategy requires more design consideration as there are no viable programs for designing these structures. Oligonucleotides have been used to create many types of structures such as nanotubes[77], tetrahedrons[78,79], icosahedrons[80], and many other polyhedral structures[6,81].

In 2010 Kim *et al.* reported a simple method of intercalating Dox into DNA tetrahedra as carriers to reverse drug resilience of cancer cells[79]. Cy5 was incorporated into the tetrahedron for characterization purpose (Figure 4-2B). Results show that even without any targeting agent, the DNA tetrahedra are able to enhance uptake and bypass the efflux process in multidrug resistant MCF-7 cancer cells.
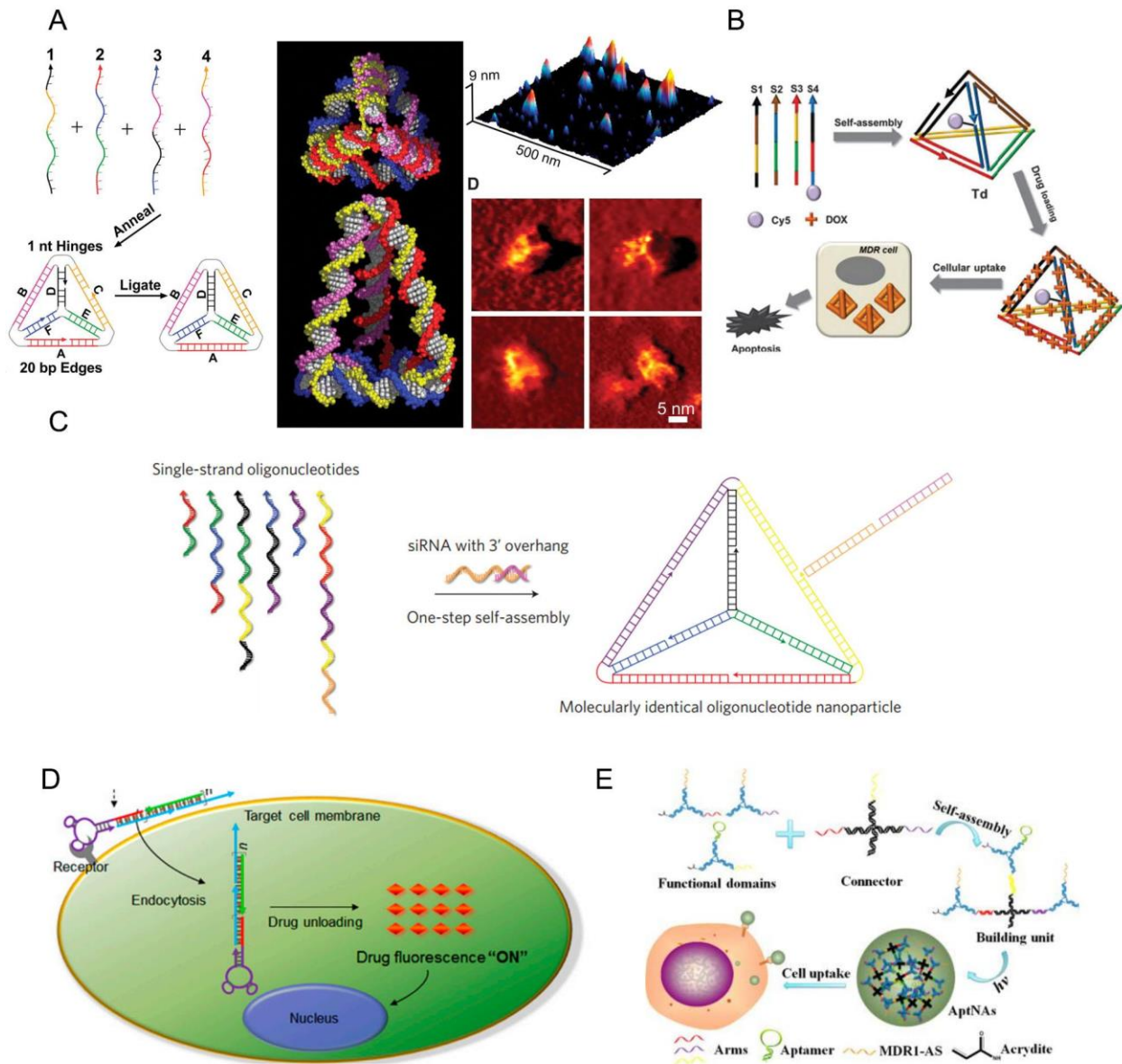
Figure 4-2 Typical examples of drug-carrying DNA nanostructures. A: The original DNA tetrahedral structure proposed by Turberfield[78]. B: Modified DNA tetrahedral structure with Cy5 dye and Dox intercalation[79]. C: Incorporation of siRNA onto the struts of the DNA nanotetrahedron[82] D: Proposed drug delivery route of DNA nanotrain[83] E: Multifunctional aptamer-based nanoparticles[84]

An example of DNA polyhedra assembled from oligonucleotides was reported by Chang *et al.* in 2011[85]. They designed a six-point-star motif with five sticky ends that are self-complementary and one end with targeting aptamer to assemble into icosahedra with diameter of around 28nm, while the ends with aptamer erect. Dox was intercalated into the structure without affecting the shape. The MUC-1 aptamer was used to target MUC 1+ MCF-7 cells. The dox-apt-icosahedron complex shows great specificity and aptamer-mediated internalization for killing epithelial cancer cells.

Lee *et al.* proposed a way to deliver siRNA using a tetrahedral DNA structure with a hydrodynamic size of 28.6 nm with narrow distribution (Figure 4-2C)[82]. Cy5-labelled such oligonucleotide particles (ONPs) with six folic acid ligands per particle were injected in nude mice with KB xenograft tumors. Results show that the ODNs accumulate primarily in the tumor and kidney. The circulation time of the ODNs is also a lot longer than the parent siRNA (blood half-life t1/2≈24.2 min vs 6 min).

A concept of nanotrain was reported by Zhu *et al.* in 2013[83]. Two strands of ODNs alternatively bind to each other triggered by an aptamer trigger to form a longer chain train-like structure with a aptamer sgc8 on one end to target specific cells (Figure 4-2D). Dox is intercalated into the DNA double strand. The complex can specifically transport the drug to target cancer cells, initiate endocytosis and unload the drugs within the cells. The complex was tested in vivo in NOD.Cg-Prkdc (scid) IL2 mice and showed reduced side effects and stronger therapeutic potency.

Wu *et al.* reported an modular aptamer based DNA nanoassembly (AptNA) approach (Figure 4-2E)[84]. Multifunctional DNA sequences are first assembled into Y shaped functional domains and then connect to X shaped connectors. The connector has a photopolymerizable arm so that the build unit with different functional domains can be polymerized into spherical structure

of diameter around 200nm. The aptamer sgc8 was used to target CCRF-CEM cancer cells. The cells shower increased viability compared to the treatment by free dox. The DNA nanoparticle also showed selectivity on CEM cells rather than the non-target Ramos cells.

Li *et al.* developed a tetrahedron motif bearing unmethylated cytosine-phosphate-guanine (CpG) motifs which have immunostimulatory properties[86]. This is due to the fact that these motifs can bind to certain cellular receptors known as endosomal Toll-like receptor 9 and trigger an immunostimulatory response. After incubation with RAW264.7 cells, these structures were mostly localized in the cytoplasm as imaged by confocal microscopy. Degradation studies were also conducted by incubating the tetrahedrons in fetal bovine serum (FBS). These structures remained stable at 4 hours whilst simple DNA duplexes degraded in the span of 2.

Sellner *et al.* reported in 2015 a *in vivo* study of gene delivery by DNA nanotubes. The nanotubes were assembled by the single stranded tile (SST) method, in which each tile consists of four 10-11 bases domains and a length of 42 bases[77]. Sticky ends of poly-As stick out of the tube side walls for functionalization. CpG and fluorescent dye ATTO488-dUTP or Cy3-dUTP are conjugated onto the structure. The in vivo study on anesthetized mice shows that while plain nanotubes do not induce an immune response, CpG conjugated nanotubes can target tissue-resident macrophages and reach intact muscle tissue almost immediately, and elevate immune response strongly. The DNA nanotubes also have some stability against DNAse I within muscle tissue.

In this chapter, we will mainly focus on the design and assembly of truncated DNA nanocages as drug delivery vehicles. Truncated nanocages are formed by the same motif that we used in chapters 2 and 3, and have the potential to be the 3rd step of CME that we are trying to mimic and study.

4.2   Results and discussion

We first used the 5-arm motif to form icosahedron. The design and sequences were the same as described in the paper by Zhang *et al.*[7] This will be the basis for subsequent structure design.(Figure 4-3) The long 5-arm center strand acts as the vertices of an icosahedron. It is named as 5v, or L in this specific design. M strands bind with one of the arm domains of L. S stands act as stick-ends, bring each 5-arm motif together. As described in the paper, the concentration of the motive needed to be limited in order for the particular shape to be formed. We characterized this design under tapping-mode AFM in air. Figure 4-4 shows flattened versions of the icosahedrons. The diameter of the particles seen in the image is about 50nm, matches our expectation for flattened particles. We then expanded the design to have more anchor points on the structure. In current design, each face of the icosahedron is hollow. The basic design goal is to replace each face with more complicated flat structures.
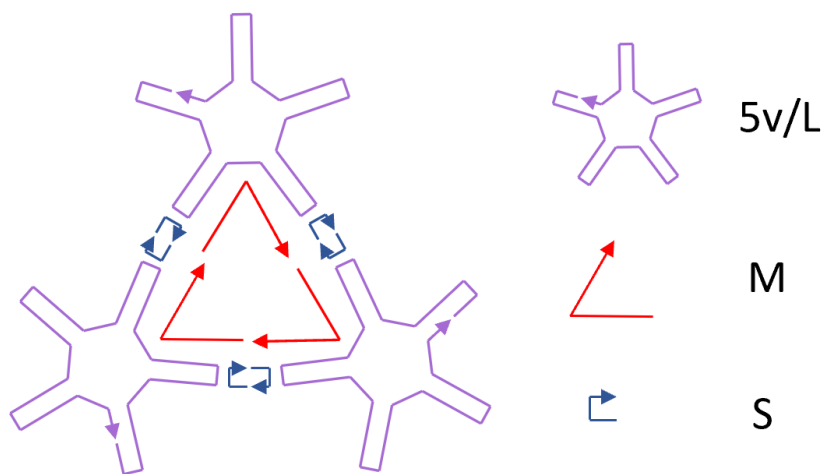
Figure 4-3 Geometric design for icosa-LMS series.
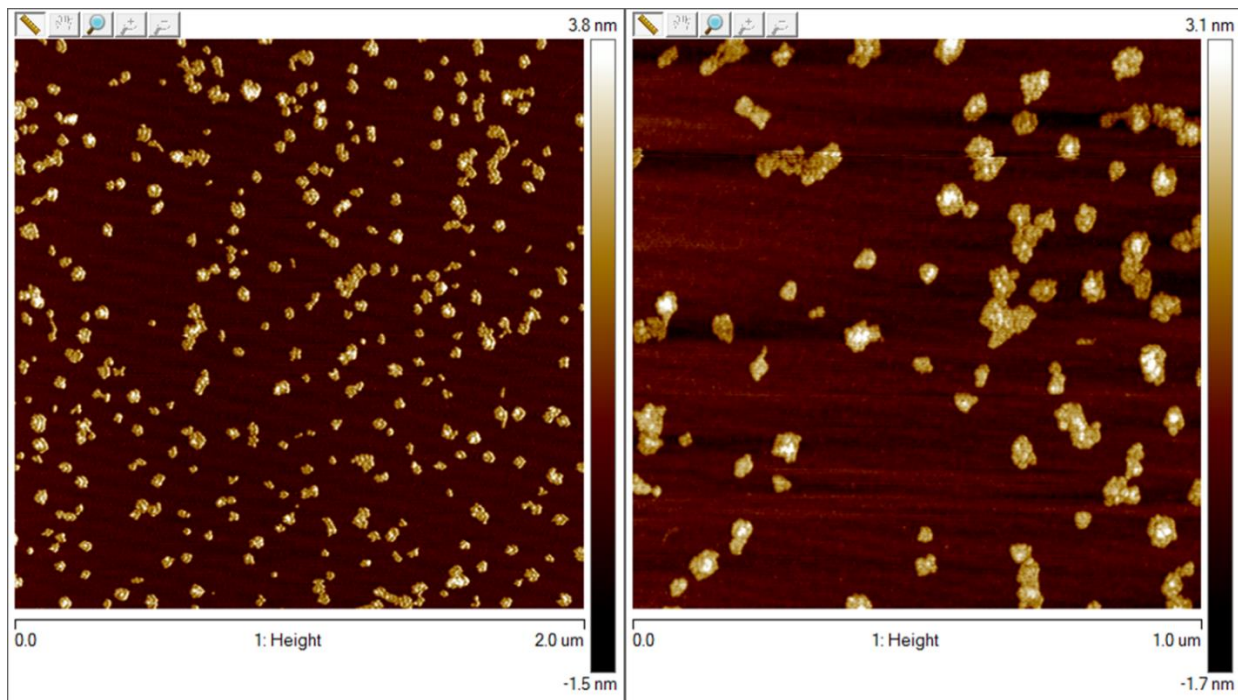
Figure 4-4 AFM results for icosa-LMS series.

Our first attempts were icosa-2 and icosa-3 series (Figure 4-5). The design principle is that by using 6-arm strands as connecting points between different faces, the distance between the 5v strands will effectively be doubled or tripled, hence expanding each face to allow more anchoring points for more functionality. In the large version, icosa-3 series, another 6-arm strand is used to maintain structural integrity of the face structure. These structures are highly symmetrical, thus the number of distinct strands is minimal.
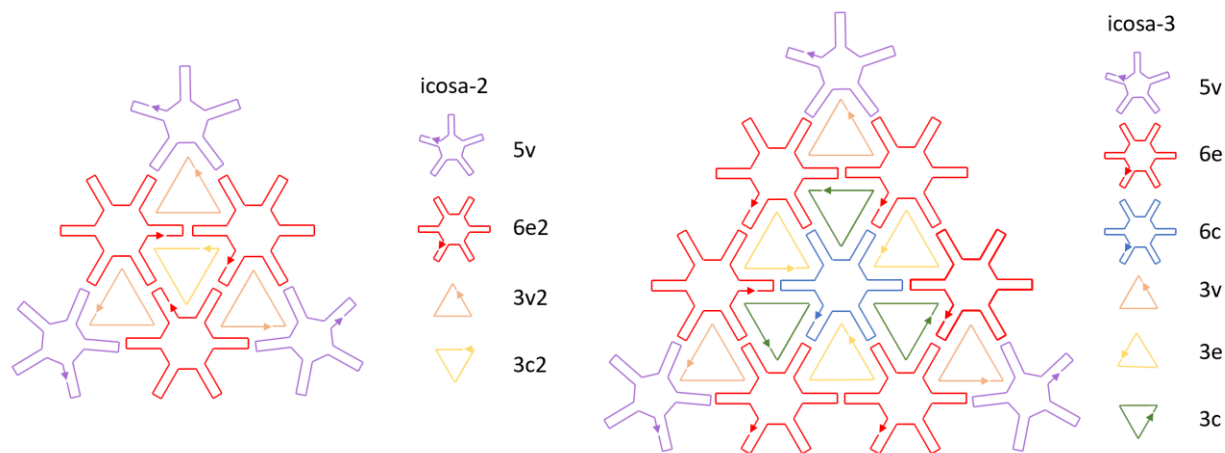
Figure 4-5 Geometric design for icosa-2 and icosa-3 series.

The structures were then characterized under AFM. (Figure 4-6,) The image shows small discrete particles with diameters of about 50nm, which is quite a bit smaller than the expected structure. We also used agarose gel to characterize the formation of icosa-2 structure, shown in Figure 4-6, right. Lane 2 and Lane 3 are supposed to be the product lanes. The molecular weight shown for these lanes did not meet our expectations. The fact that the bands in lane 1 and 2 are smeared also showed that there were a range of different structures formed, instead of one distinct structure that we desired. We attributed this phenomenon to the long 6e strands, because the linkage between the face motifs may not have occurred in the way that we expected, and that would result in dimers, trimers or other multimers.
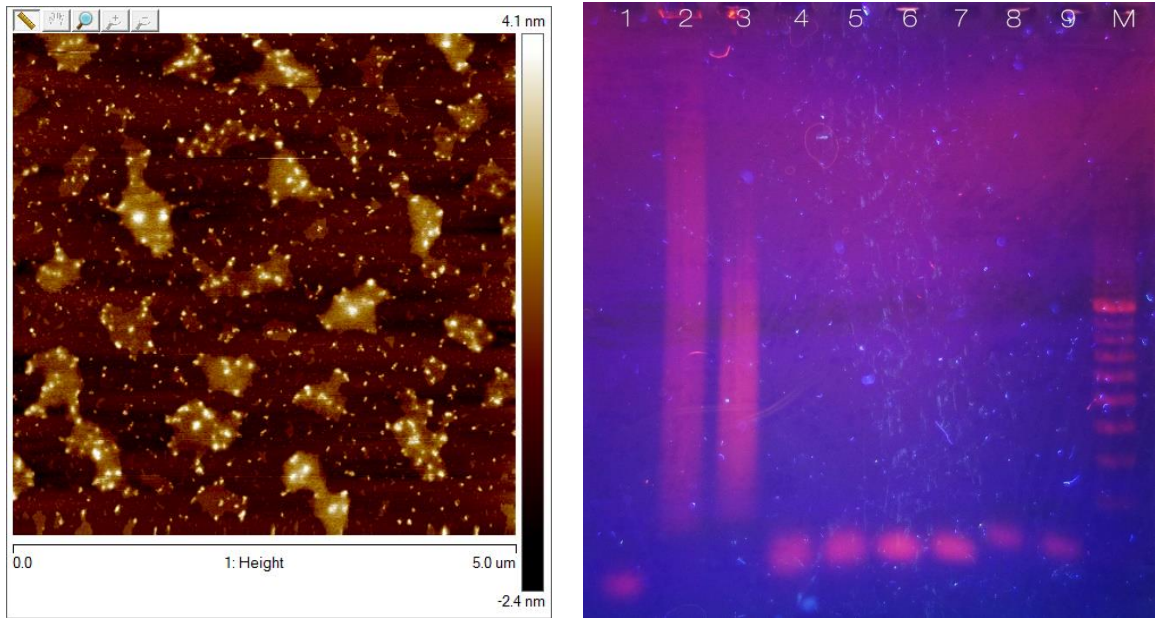
Figure 4-6 Left: AFM scan of icosa-2 series. Right: 0.5% agarose gel.
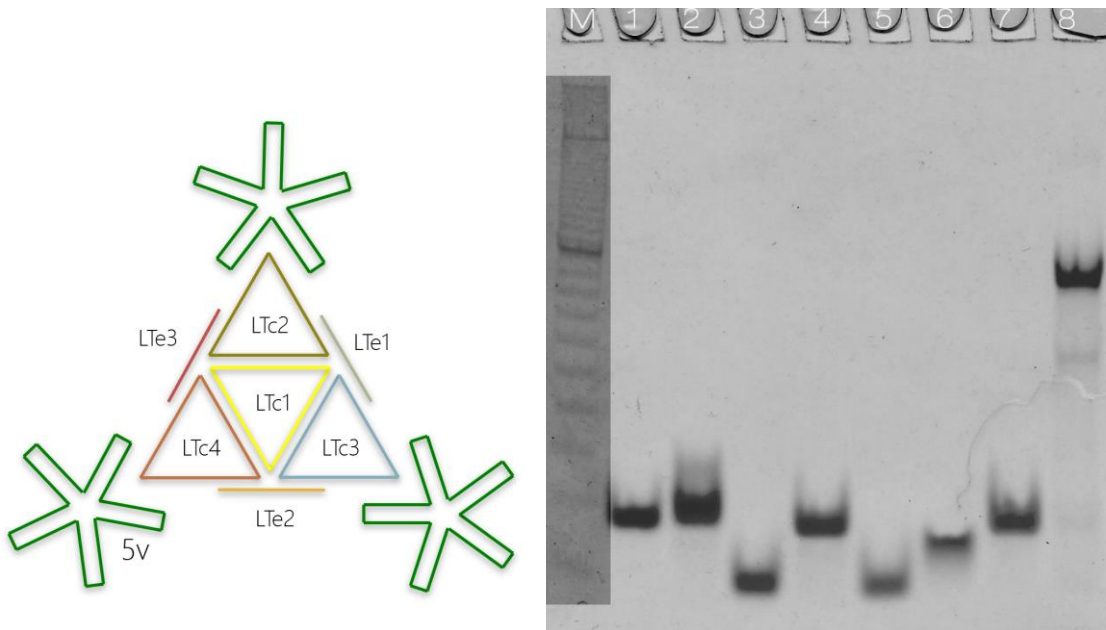
Figure 4-7 Left: Geometric design for icosa-LT series. Right: 5% PAGE gel to show the formation of the face motif. Lane1-7 are individual component strands. Lane 8 is the product lane.

At this point in the experiment, we realized that too much symmetry may cause the formation of unwanted structures. Thus, we switched the design focus to constructing a face structure that is non-symmetric. The icosa-LT series is a product of this idea. Figure 4-7 left shows the design of the structure. It consists of 7 distinct DNA strands. PAGE gel also showed promising results. The product lane 8 showed a very sharp band, indicating the successful formation of the face motif. AFM images also showed uniform sizes of the particles formed. However, when put together with 5v strand, there were no large particle observed. Instead, the AFM image showed a morphology possibly formed by merely interconnecting each face motif. Further work is needed to finetune the conditions to facilitate the formation of icosahedron.

4.3 Conclusion

In this chapter we explored different designs of potential truncated icosahedron structures. The focus was on designing a face structure that is robust and can also form truncated structure with the 5v strand. We experimented with 5 different designs of structures, and found out that excessive symmetry may not be desirable under this circumstance. A non-symmetric face structure was successfully designed and synthetized, yet the combination of this motif to the 5v strands was not successful. This work explored possible avenues for expanding the size and functionality of truncated icosahedral structures. The icosa-LT structure can potentially be used to construct icosahedral structure if the conditions are finetuned.

Chapter 4, in part, is a reprint of the material as it appears in "DNA Nanotechnology for Precise Control over Drug Delivery and Gene Therapy", *Small*, **2016**, 12(9), 1117-1132, with the coauthors of C. Angell, L. Zhang, Y. Chen. The dissertation author is the co-first author of this work.

CHAPTER 5: CONCLUSIONS

In this dissertation, we established a path to mimicking clathrin-mediated endocytosis using DNA nanostructures. Using DNA as a highly programmable and functionalizable material, we were able to design effective mechanisms to mimic different stages of CME.

In the first part we successfully designed a 3-arm motif that can self-assemble into arrays while anchored into a supported lipid bilayer. These arrays mimic the morphology and functionality of large-scale clathrin patches on cell surfaces. The structure is also tunable in the size of the repeat units, and can be integrated with other nanoparticles. The applications can thus be expanded to other fields.

In the second part we designed a reversible transformation mechanism that utilizes fuel strand replacement and hairpin structure formation. We further applied this mechanism to an array-forming 3-arm motif, to create an array-to-particle transformation that mimics the transformation stage of CME. This reversible transformation mechanism can also be used in many other DNA machines.

In the third part we explored possible designs of creating truncated DNA nanoparticles. We found that symmetry may induce unwanted structures, and we designed a non-symmetric face motif that can potentially be integrated into drug delivery vehicle design using DNA nanotechnology.

The work described in this dissertation led us closer to mimicking CME using DNA nanostructures, and understanding more about the process. The mechanisms and design principles utilized in this work also have wide implications for other fields.

REFERENCES

1. Angell, C., Xie, S., Zhang, L. & Chen, Y. DNA Nanotechnology for Precise Control over Drug Delivery and Gene Therapy. *Small* **12**, 1117–1132 (2016).

2. Seeman, N. C. & Kallenbach, N. R. Design of immobile nucleic acid junctions. *Biophysical Journal* **44**, 201–209 (1983).

3. Douglas, S. M., Marblestone, A. H., Teerapittayanon, S., Vazquez, A., Church, G. M. & Shih, W. M. Rapid prototyping of 3D DNA-origami shapes with caDNAno. *Nucl. Acids Res.* gkp436 (2009) doi:10.1093/nar/gkp436.

4. Goodman, R. P., Schaap, I. a. T., Tardin, C. F., Erben, C. M., Berry, R. M., Schmidt, C. F. & Turberfield, A. J. Rapid Chiral Assembly of Rigid DNA Building Blocks for Molecular Nanofabrication. *Science* **310**, 1661–1665 (2005).

5. He, Y., Chen, Y., Liu, H., Ribbe, A. E. & Mao, C. Self-Assembly of Hexagonal DNA Two-Dimensional (2D) Arrays. *J. Am. Chem. Soc.* **127**, 12202–12203 (2005).

6. He, Y., Ye, T., Su, M., Zhang, C., Ribbe, A. E., Jiang, W. & Mao, C. Hierarchical self-assembly of DNA into symmetric supramolecular polyhedra. *Nature* **452**, 198–201 (2008).

7. Zhang, C., Su, M., He, Y., Zhao, X., Fang, P., Ribbe, A. E., Jiang, W. & Mao, C. Conformational flexibility facilitates self-assembly of complex DNA nanostructures. *PNAS* **105**, 10665–10669 (2008).

8. Ke, Y., Ong, L. L., Shih, W. M. & Yin, P. Three-Dimensional Structures Self-Assembled from DNA Bricks. *Science* **338**, 1177–1183 (2012).

9. Chen, J. & Seeman, N. C. Synthesis from DNA of a molecule with the connectivity of a cube. *Nature* **350**, 631–633 (1991).

10. Rothemund, P. W. K. Folding DNA to create nanoscale shapes and patterns. *Nature* **440**, 297–302 (2006).

11. Douglas, S. M., Dietz, H., Liedl, T., Högberg, B., Graf, F. & Shih, W. M. Self-assembly of DNA into nanoscale three-dimensional shapes. *Nature* **459**, 414–418 (2009).

12. Andersen, E. S., Dong, M., Nielsen, M. M., Jahn, K., Lind-Thomsen, A., Mamdouh, W., Gothelf, K. V., Besenbacher, F. & Kjems, J. DNA Origami Design of Dolphin-Shaped Structures with Flexible Tails. *ACS Nano* **2**, 1213–1218 (2008).

13. Marras, A. E., Zhou, L., Su, H.-J. & Castro, C. E. Programmable motion of DNA origami mechanisms. *PNAS* **112**, 713–718 (2015).

14. Shih, W. M., Quispe, J. D. & Joyce, G. F. A 1.7-kilobase single-stranded DNA that folds into a nanoscale octahedron. *Nature* **427**, 618–621 (2004).

15. Tørring, T., Voigt, N. V., Nangreave, J., Yan, H. & Gothelf, K. V. DNA origami: a quantum leap for self-assembly of complex structures. *Chem. Soc. Rev.* **40**, 5636–5646 (2011).

16. Smith, D. M., Schü, Ller, V., Forthmann, C., Schreiber, R., Tinnefeld, P. & Liedl, T. A Structurally Variable Hinged Tetrahedron Framework from DNA Origami. *Journal of Nucleic Acids* **2011**, e360954 (2011).

17. Zhao, Y.-X., Shaw, A., Zeng, X., Benson, E., Nyström, A. M. & Högberg, B. DNA Origami Delivery System for Cancer Therapy with Tunable Release Properties. *ACS Nano* **6**, 8684–8691 (2012).

18. Zhang, Q., Jiang, Q., Li, N., Dai, L., Liu, Q., Song, L., Wang, J., Li, Y., Tian, J., Ding, B. & Du, Y. DNA Origami as an In Vivo Drug Delivery Vehicle for Cancer Therapy. *ACS Nano* **8**, 6633–6643 (2014).

19. Sobczak, J.-P. J., Martin, T. G., Gerling, T. & Dietz, H. Rapid Folding of DNA into Nanoscale Shapes at Constant Temperature. *Science* **338**, 1458–1461 (2012).

20. Iinuma, R., Ke, Y., Jungmann, R., Schlichthaerle, T., Woehrstein, J. B. & Yin, P. Polyhedra Self-Assembled from DNA Tripods and Characterized with 3D DNA-PAINT. *Science* **344**, 65–69 (2014).

21. Tourdot, R. & Radhakrishnan, R. Clathrin Mediated Endocytosis and its Role in Viral Entry. *Atlas of Genetics and Cytogenetics in Oncology and Haematology* (2013).

22. Henne, W. M., Boucrot, E., Meinecke, M., Evergren, E., Vallis, Y., Mittal, R. & McMahon, H. T. FCHo Proteins Are Nucleators of Clathrin-Mediated Endocytosis. *Science* **328**, 1281–1284 (2010).

23. Benmerah, A., Lamaze, C., Bègue, B., Schmid, S. L., Dautry-Varsat, A. & Cerf-Bensussan, N. AP-2/Eps15 Interaction Is Required for Receptor-mediated Endocytosis. *Journal of Cell Biology* **140**, 1055–1062 (1998).

24. Rappoport, J. Z., Kemal, S., Benmerah, A. & Simon, S. M. Dynamics of clathrin and adaptor proteins during endocytosis. *American Journal of Physiology-Cell Physiology* **291**, C1072–C1081 (2006).

25.   Avinoam, O., Schorb, M., Beese, C. J., Briggs, J. A. G. & Kaksonen, M. Endocytic sites mature by continuous bending and remodeling of the clathrin coat. *Science* **348**, 1369–1372 (2015).

26.   Wakeham, D. E., Chen, C.-Y., Greene, B., Hwang, P. K. & Brodsky, F. M. Clathrin self-assembly involves coordinated weak interactions favorable for cellular regulation. *The EMBO Journal* **22**, 4980–4990 (2003).

27.   Fotin, A., Cheng, Y., Sliz, P., Grigorieff, N., Harrison, S. C., Kirchhausen, T. & Walz, T. Molecular model for a complete clathrin lattice from electron cryomicroscopy. *Nature* **432**, 573–579 (2004).

28.   Kirchhausen, T., Scarmato, P., Harrison, S. C., Monroe, J. J., Chow, E. P., Mattaliano, R. J., Ramachandran, K. L., Smart, J. E., Ahn, A. H. & Brosius, J. Clathrin light chains LCA and LCB are similar, polymorphic, and share repeated heptad motifs. *Science* **236**, 320–324 (1987).

29.   Seeman, N. C. DNA in a material world. *Nature* **421**, 427–431 (2003).

30.   Yin, P., Hariadi, R. F., Sahu, S., Choi, H. M. T., Park, S. H., LaBean, T. H. & Reif, J. H. Programming DNA Tube Circumferences. *Science* **321**, 824–826 (2008).

31.   Yan, H., Park, S. H., Finkelstein, G., Reif, J. H. & LaBean, T. H. DNA-Templated Self-Assembly of Protein Arrays and Highly Conductive Nanowires. *Science* **301**, 1882–1884 (2003).

32.   Rothemund, P. W. K., Ekani-Nkodo, A., Papadakis, N., Kumar, A., Fygenson, D. K. & Winfree, E. Design and Characterization of Programmable DNA Nanotubes. *J. Am. Chem. Soc.* **126**, 16344–16352 (2004).

33.   Yurke, B., Turberfield, A. J., Mills, A. P., Simmel, F. C. & Neumann, J. L. A DNA-fuelled molecular machine made of DNA. *Nature* **406**, 605–608 (2000).

34.   Yan, H., Zhang, X., Shen, Z. & Seeman, N. C. A robust DNA mechanical device controlled by hybridization topology. *Nature* **415**, 62–65 (2002).

35.   Liu, M., Fu, J., Hejesen, C., Yang, Y., Woodbury, N. W., Gothelf, K., Liu, Y. & Yan, H. A DNA tweezer-actuated enzyme nanoreactor. *Nature Communications* **4**, 2127 (2013).

36.   Ke, Y., Meyer, T., Shih, W. M. & Bellot, G. Regulation at a distance of biomolecular interactions using a DNA origami nanoactuator. *Nature Communications* **7**, 10935 (2016).

37.   Sherman, W. B. & Seeman, N. C. A Precisely Controlled DNA Biped Walking Device. *Nano Lett.* **4**, 1203–1207 (2004).

38.   Yin, P., Yan, H., Daniell, X. G., Turberfield, A. J. & Reif, J. H. A Unidirectional DNA Walker That Moves Autonomously along a Track. *Angewandte Chemie International Edition* **43**, 4906–4911 (2004).

39.   Omabegho, T., Sha, R. & Seeman, N. C. A Bipedal DNA Brownian Motor with Coordinated Legs. *Science* **324**, 67–71 (2009).

40.   Yin, P., Choi, H. M. T., Calvert, C. R. & Pierce, N. A. Programming biomolecular self-assembly pathways. *Nature* **451**, 318–322 (2008).

41.   Lund, K., Manzo, A. J., Dabby, N., Michelotti, N., Johnson-Buck, A., Nangreave, J., Taylor, S., Pei, R., Stojanovic, M. N., Walter, N. G., Winfree, E. & Yan, H. Molecular robots guided by prescriptive landscapes. *Nature* **465**, 206–210 (2010).

42.   Bockelmann, U., Essevaz-Roulet, B. & Heslot, F. Molecular Stick-Slip Motion Revealed by Opening DNA with Piconewton Forces. *Phys. Rev. Lett.* **79**, 4489–4492 (1997).

43.   Garcia-Manyes, S. & Sanz, F. Nanomechanics of lipid bilayers by force spectroscopy with AFM: A perspective. *Biochimica et Biophysica Acta (BBA) - Biomembranes* **1798**, 741–749 (2010).

44.   Langer, R. New methods of drug delivery. *Science* **249**, 1527–1533 (1990).

45.   Langer, R. Drug delivery and targeting. *Nature* **392**, 5–10 (1998).

46.   Spira, A., Beane, J. E., Shah, V., Steiling, K., Liu, G., Schembri, F., Gilman, S., Dumas, Y.-M., Calner, P., Sebastiani, P., Sridhar, S., Beamis, J., Lamb, C., Anderson, T., Gerry, N., Keane, J., Lenburg, M. E. & Brody, J. S. Airway epithelial gene expression in the diagnostic evaluation of smokers with suspect lung cancer. *Nature Medicine* **13**, 361–366 (2007).

47.   Hu, C.-M. J., Zhang, L., Aryal, S., Cheung, C., Fang, R. H. & Zhang, L. Erythrocyte membrane-camouflaged polymeric nanoparticles as a biomimetic delivery platform. *PNAS* **108**, 10980–10985 (2011).

48.   Felgner, P. L. & Ringold, G. M. Cationic liposome-mediated transfection. *Nature* **337**, 387–388 (1989).

49.   Torchilin, V. P. Recent advances with liposomes as pharmaceutical carriers. *Nat Rev Drug Discov* **4**, 145–160 (2005).

50.   Alexis, F., Pridgen, E., Molnar, L. K. & Farokhzad, O. C. Factors Affecting the Clearance and Biodistribution of Polymeric Nanoparticles. *Mol. Pharmaceutics* **5**, 505–515 (2008).

51.   Sun, T., Zhang, Y. S., Pang, B., Hyun, D. C., Yang, M. & Xia, Y. Engineered Nanoparticles for Drug Delivery in Cancer Therapy. *Angew. Chem. Int. Ed.* **53**, 12320–12364 (2014).

52.   Farokhzad, O. C. & Langer, R. Impact of Nanotechnology on Drug Delivery. *ACS Nano* **3**, 16–20 (2009).

53.   Peer, D., Karp, J. M., Hong, S., Farokhzad, O. C., Margalit, R. & Langer, R. Nanocarriers as an emerging platform for cancer therapy. *Nat Nano* **2**, 751–760 (2007).

54.   Geng, Y., Dalhaimer, P., Cai, S., Tsai, R., Tewari, M., Minko, T. & Discher, D. E. Shape effects of filaments versus spherical particles in flow and drug delivery. *Nat Nano* **2**, 249–255 (2007).

55.   Champion, J. A. & Mitragotri, S. Role of target geometry in phagocytosis. *PNAS* **103**, 4930–4934 (2006).

56.   Sun, W., Jiang, T., Lu, Y., Reiff, M., Mo, R. & Gu, Z. Cocoon-Like Self-Degradable DNA Nanoclew for Anticancer Drug Delivery. *J. Am. Chem. Soc.* **136**, 14722–14725 (2014).

57.   Agudelo, D., Bourassa, P., Bérubé, G. & Tajmir-Riahi, H.-A. Intercalation of antitumor drug doxorubicin and its analogue by DNA duplex: Structural features and biological implications. *International Journal of Biological Macromolecules* **66**, 144–150 (2014).

58.   Surana, S., Bhat, J. M., Koushika, S. P. & Krishnan, Y. An autonomous DNA nanomachine maps spatiotemporal pH changes in a multicellular living organism. *Nat Commun* **2**, 340 (2011).

59.   Zhu, G., Cansiz, S., You, M., Qiu, L., Han, D., Zhang, L., Mei, L., Fu, T., Chen, Z. & Tan, W. Nuclease-resistant synthetic drug-DNA adducts: programmable drug-DNA conjugation for targeted anticancer drug delivery. *NPG Asia Mater* **7**, e169 (2015).

60.   Fellmann, C. & Lowe, S. W. Stable RNA interference rules for silencing. *Nat Cell Biol* **16**, 10–18 (2014).

61.   Naito, Y. & Ui-Tei, K. siRNA design software for a target gene-specific RNA interference. *Front. Gene.* **3**, 102 (2012).

62.   Castanotto, D. & Rossi, J. J. The promises and pitfalls of RNA-interference-based therapeutics. *Nature* **457**, 426–433 (2009).

63.   Guo, P., Coban, O., Snead, N. M., Trebley, J., Hoeprich, S., Guo, S. & Shu, Y. Engineering RNA for Targeted siRNA Delivery and Medical Application. *Advanced Drug Delivery Reviews* **62**, 650–666 (2010).

64.   Liu, L., Xu, K., Wang, H., Tan, P. K. J., Fan, W., Venkatraman, S. S., Li, L. & Yang, Y.-Y. Self-assembled cationic peptide nanoparticles as an efficient antimicrobial agent. *Nat Nano* **4**, 457–463 (2009).

65.   Wilner, O. I. & Willner, I. Functionalized DNA Nanostructures. *Chem. Rev.* **112**, 2528–2556 (2012).

66.   Allen, T. M. Ligand-targeted therapeutics in anticancer therapy. *Nat Rev Cancer* **2**, 750–763 (2002).

67.   Cheng, E., Xing, Y., Chen, P., Yang, Y., Sun, Y., Zhou, D., Xu, L., Fan, Q. & Liu, D. A pH-Triggered, Fast-Responding DNA Hydrogel. *Angewandte Chemie* **121**, 7796–7799 (2009).

68.   Modi, S., G, S. M., Goswami, D., Gupta, G. D., Mayor, S. & Krishnan, Y. A DNA nanomachine that maps spatial and temporal pH changes inside living cells. *Nat Nano* **4**, 325–330 (2009).

69.   Lühmann, T., Rimann, M., Bittermann, A. G. & Hall, H. Cellular Uptake and Intracellular Pathways of PLL-g-PEG-DNA Nanoparticles. *Bioconjugate Chem.* **19**, 1907–1916 (2008).

70.   Chen, G., Liu, D., He, C., Gannett, T. R., Lin, W. & Weizmann, Y. Enzymatic Synthesis of Periodic DNA Nanoribbons for Intracellular pH Sensing and Gene Silencing. *J. Am. Chem. Soc.* **137**, 3844–3851 (2015).

71.   Xiang, S., Tong, H., Shi, Q., Fernandes, J. C., Jin, T., Dai, K. & Zhang, X. Uptake mechanisms of non-viral gene delivery. *Journal of Controlled Release* **158**, 371–378 (2012).

72.   Chen, X., Shank, S., Davis, P. B. & Ziady, A. G. Nucleolin-Mediated Cellular Trafficking of DNA Nanoparticle Is Lipid Raft and Microtubule Dependent and Can Be Modulated by Glucocorticoid. *Mol Ther* **19**, 93–102 (2011).

73.   Dalby, B., Cates, S., Harris, A., Ohki, E. C., Tilkins, M. L., Price, P. J. & Ciccarone, V. C. Advanced transfection with Lipofectamine 2000 reagent: primary neurons, siRNA, and high-throughput applications. *Methods* **33**, 95–103 (2004).

74.   Ke, Y., Bellot, G., Voigt, N. V., Fradkov, E. & Shih, W. M. Two design strategies for enhancement of multilayer–DNA-origami folding: underwinding for specific intercalator rescue and staple-break positioning. *Chem. Sci.* **3**, 2587–2597 (2012).

75.   Mikkilä, J., Eskelinen, A.-P., Niemelä, E. H., Linko, V., Frilander, M. J., Törmä, P. & Kostiainen, M. A. Virus-Encapsulated DNA Origami Nanostructures for Cellular Delivery. *Nano Lett.* **14**, 2196–2200 (2014).

76.   Kim, M.-G., Park, J. Y., Shim, G., Choi, H.-G. & Oh, Y.-K. Biomimetic DNA nanoballs for oligonucleotide delivery. *Biomaterials* **62**, 155–163 (2015).

77.   Sellner, S., Kocabey, S., Nekolla, K., Krombach, F., Liedl, T. & Rehberg, M. DNA nanotubes as intracellular delivery vehicles in vivo. *Biomaterials* **53**, 453–463 (2015).

78.   Goodman, R. P., Berry, R. M. & Turberfield, A. J. The single-step synthesis of a DNA tetrahedron. *Chem. Commun.* 1372–1373 (2004) doi:10.1039/B402293A.

79.   Kim, K.-R., Kim, D.-R., Lee, T., Yhee, J. Y., Kim, B.-S., Kwon, I. C. & Ahn, D.-R. Drug delivery by a self-assembled DNA tetrahedron for overcoming drug resistance in breast cancer cells. *Chem. Commun.* **49**, 2010–2012 (2013).

80.   Bhatia, D., Mehtab, S., Krishnan, R., Indi, S. S., Basu, A. & Krishnan, Y. Icosahedral DNA Nanocapsules by Modular Assembly. *Angewandte Chemie International Edition* **48**, 4134–4137 (2009).

81.   Zhang, Y. & Seeman, N. C. Construction of a DNA-Truncated Octahedron. *J. Am. Chem. Soc.* **116**, 1661–1669 (1994).

82.   Lee, H., Lytton-Jean, A. K. R., Chen, Y., Love, K. T., Park, A. I., Karagiannis, E. D., Sehgal, A., Querbes, W., Zurenko, C. S., Jayaraman, M., Peng, C. G., Charisse, K., Borodovsky, A., Manoharan, M., Donahoe, J. S., Truelove, J., Nahrendorf, M., Langer, R. & Anderson, D. G. Molecularly self-assembled nucleic acid nanoparticles for targeted in vivo siRNA delivery. *Nat Nano* **7**, 389–393 (2012).

83.   Zhu, G., Zheng, J., Song, E., Donovan, M., Zhang, K., Liu, C. & Tan, W. Self-assembled, aptamer-tethered DNA nanotrains for targeted transport of molecular drugs in cancer theranostics. *PNAS* **110**, 7998–8003 (2013).

84.   Wu, C., Han, D., Chen, T., Peng, L., Zhu, G., You, M., Qiu, L., Sefah, K., Zhang, X. & Tan, W. Building a Multifunctional Aptamer-Based DNA Nanoassembly for Targeted Cancer Therapy. *J. Am. Chem. Soc.* **135**, 18644–18650 (2013).

85.   Chang, M., Yang, C.-S. & Huang, D.-M. Aptamer-Conjugated DNA Icosahedral Nanoparticles As a Carrier of Doxorubicin for Cancer Therapy. *ACS Nano* **5**, 6156–6163 (2011).

86.   Li, J., Pei, H., Zhu, B., Liang, L., Wei, M., He, Y., Chen, N., Li, D., Huang, Q. & Fan, C. Self-Assembled Multivalent DNA Nanostructures for Noninvasive Intracellular Delivery of Immunostimulatory CpG Oligonucleotides. *ACS Nano* **5**, 8783–8789 (2011).